Supplementary Material

Experimental time courses

Supplementary Tables 1, 2 show the number of samples for each time point in the experimental time courses.

Tables 1: Tables summarising the number of samples for each time point in the ileal experimental time courses.

(a) BrdU (control)

Time	N. Samples
30 min	36
45 min	28
1 h	21
2 h	28
6 h	57
10 h	33
18 h	18
21 h	27
1 d	30
1 d 3 h	22
1 d 8 h	24

(b) Acute injury

Time	N. Samples
1 h	80
1 h 28 min	22
1 h 30 min	30
3 h 27 min	39
4 h 1 min	28
6 h	30
12 h	30
1 d	26

(c) Chronic injury

Time	N. Samples
1 h	30
2 h	30
8 h	30
14 h	17
15 h 20 min	30
17 h 35 min	30
1 d	23
1 d 17 h 5 min	30
1 d 17 h 35 min	30
1 d 18 h	25
2 d	30

Tables 2: Tables summarising the number of samples for each time point in the duodenal experimental time courses.

(a) BrdU (control)

Time	N. Samples
1 h	20
12 h	20
1 d	16
1 d 8 h	18

(b) Acute injury

Time	N. Samples
1 h	30
1 h 30 min	30
6 h	27
12 h	23
1 d	25

(c) Chronic injury

Time	N. Samples
1 h	30
2 h	30
8 h	30
14 h	17
15 h 20 min	30
17 h 35 min	30
1 d	30
1 d 17 h 5 min	30
1 d 17 h 35 min	30
1 d 18 h	23
2 d	30

Time series simulated by applying the cell-based model

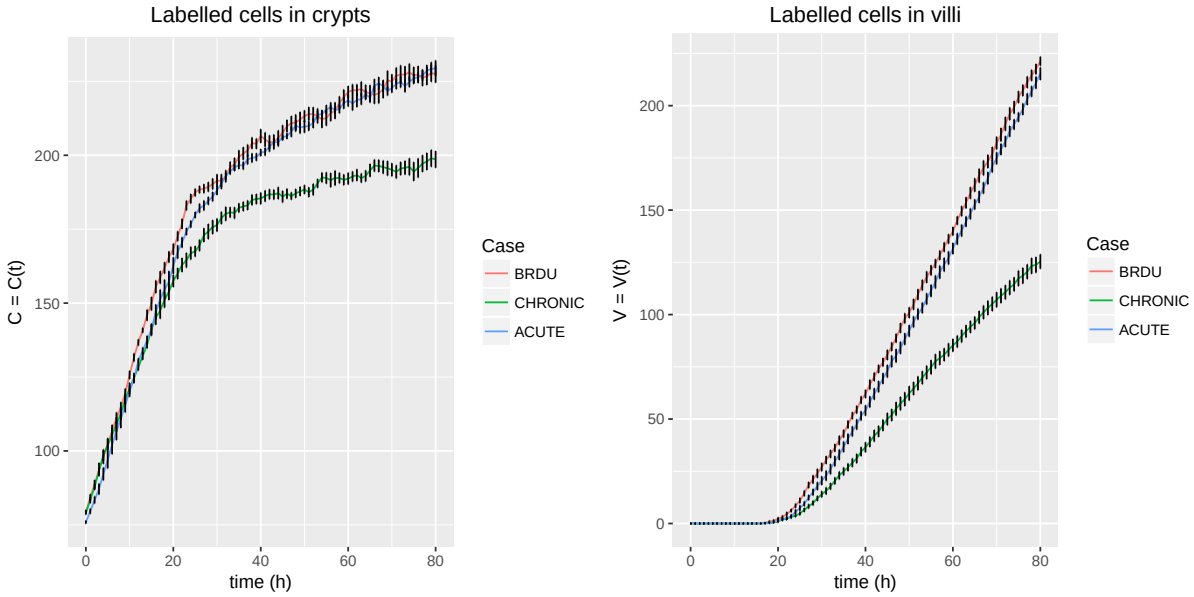

Figure 1: **Time series simulated by applying the cell-based model**. Time series representing average numbers of simulated labelled cells in crypts and villi during acute injury, chronic injury and BrdU (control). Averages were calculated from 10 simulations for each condition. Error bars indicate standard errors.

Posterior predictive distributions

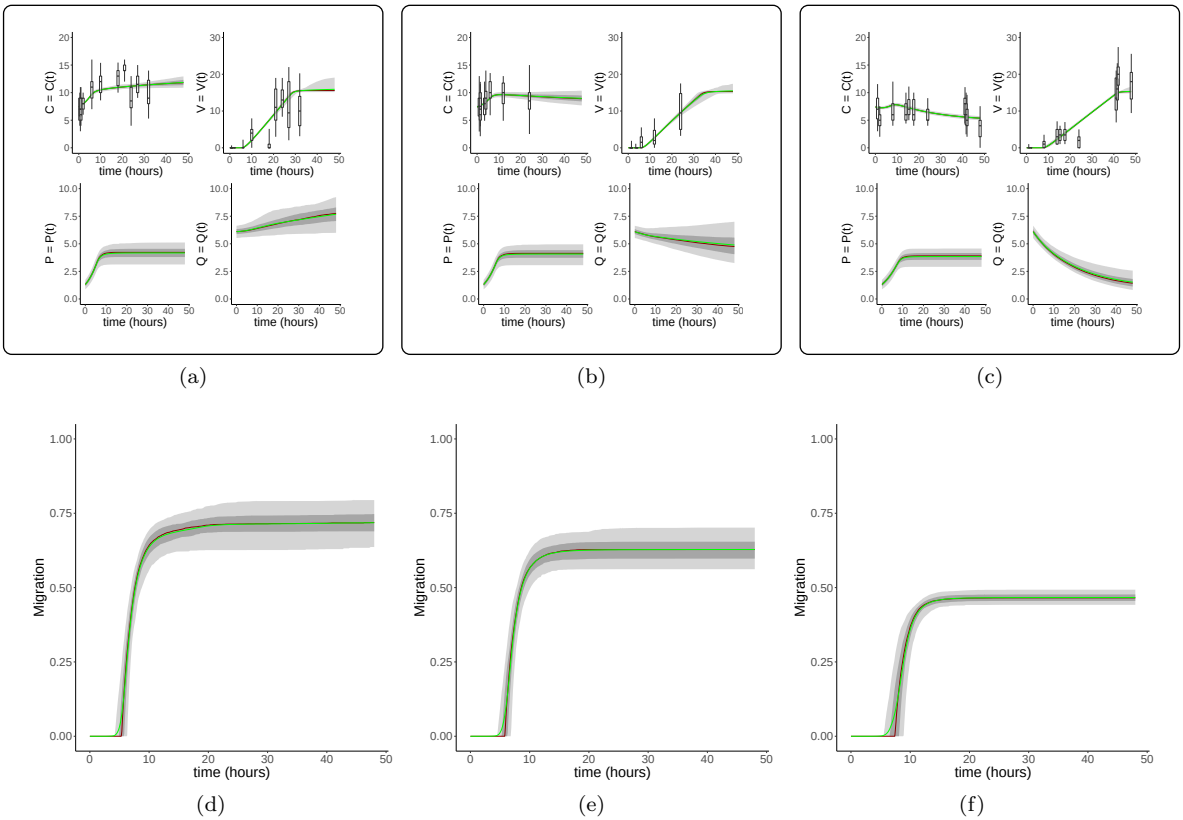

Figure 2: **Fits of the three-compartment model to ileal time course data**. (a)-(b)-(c) Posterior predictive distributions and estimates of parameter uncertainty obtained by fitting the three-compartment model (Eqs. (2)) against ileal time courses. Posterior predictive distributions inferred from (a) BrdU (control), (b) acute injury, (c) chronic injury experimental time courses. Boxplots represent the 0.05, 0.25, 0.75, 0.95 quantiles of the experimental data. Grey area plots represent the 0.05, 0.25, 0.75, 0.95 quantiles of the posterior predictive distributions (red line: posterior median; green line: posterior mean). (d)-(e)-(f) Plots representing the posterior predictive distribution of the migration term $\gamma_v(P-P^*)H(P-P^*)+\gamma_v(Q-Q^*)H(Q-Q^*)$ in the ileum obtained from control (BrdU) (d), acute injury (e) and chronic injury (f) time courses. The contribution to migration is reduced during chronic injury.

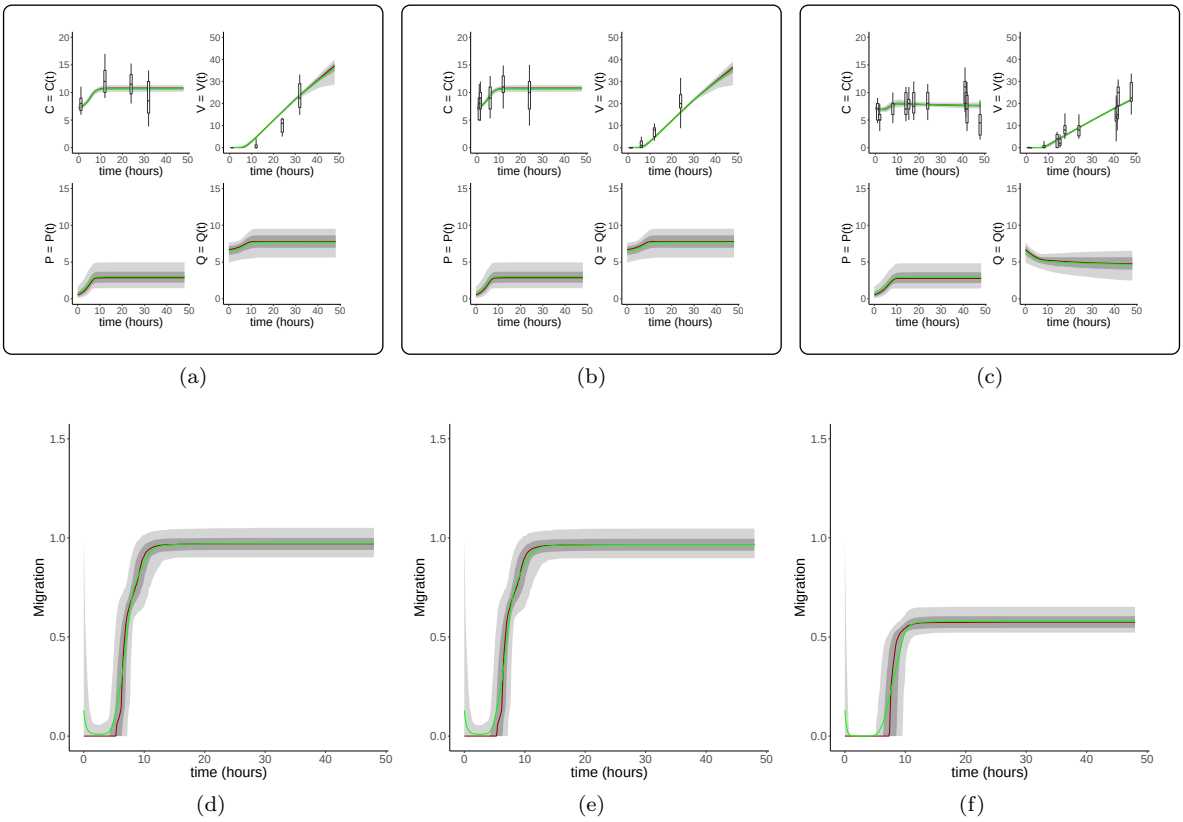

Figure 3: **Fits of the three-compartment model to duodenal time course data**. (a)-(b)-(c) Posterior predictive distributions and estimates of parameter uncertainty obtained by fitting the three-compartment model (Eqs. (2)) against duodenal time courses. Posterior predictive distributions inferred from (a) BrdU (control), (b) acute injury, (c) chronic injury experimental time courses. Boxplots represent the 0.05, 0.25, 0.75, 0.95 quantiles of the experimental data. Grey area plots represent the 0.05, 0.25, 0.75, 0.95 quantiles of the posterior predictive distributions (red line: posterior median; green line: posterior mean). (d)-(e)-(f) Plots representing the posterior predictive distribution of the migration term $\gamma_v(P-P^*)H(P-P^*)+\gamma_v(Q-Q^*)H(Q-Q^*)$ in the duodenum obtained from control (BrdU) (d), acute injury (e) and chronic injury (f) time courses. The contribution to migration is reduced during chronic injury.

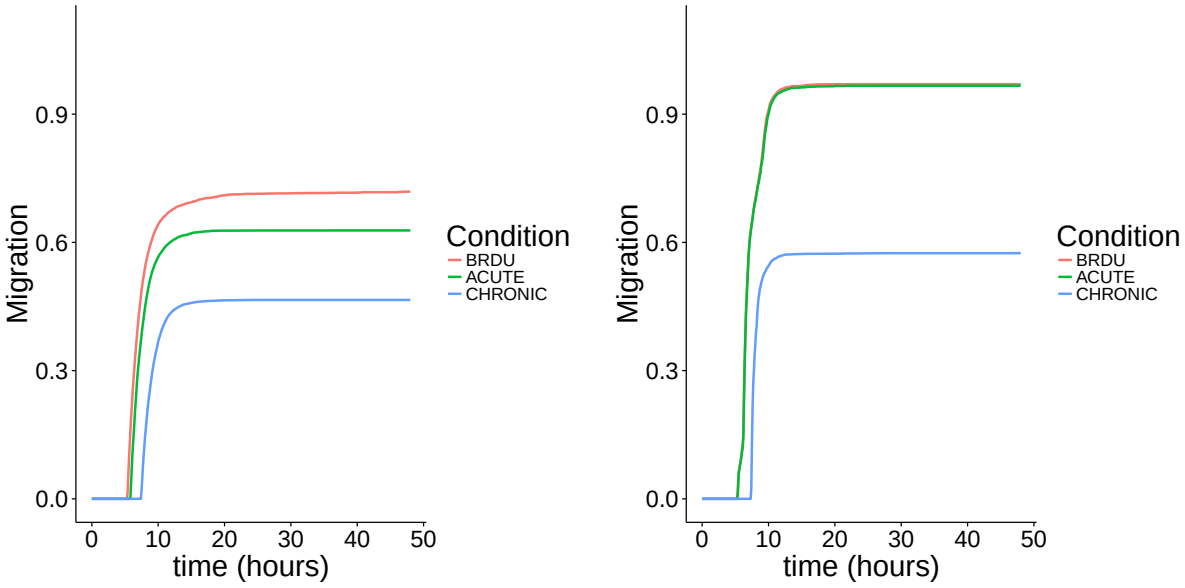

(a) (b)

Figure 4: **Migration terms of the three-compartment model when fitted against experimental time courses**. Plots representing the medians of the posterior predictive distribution of the migration terms $\gamma_v(P - P^*)H(P - P^*) + \gamma_v(Q - Q^*)H(Q - Q^*)$ in ileum (a) and in duodenum (b). Contribution to migration is reduced during simulated chronic injury.

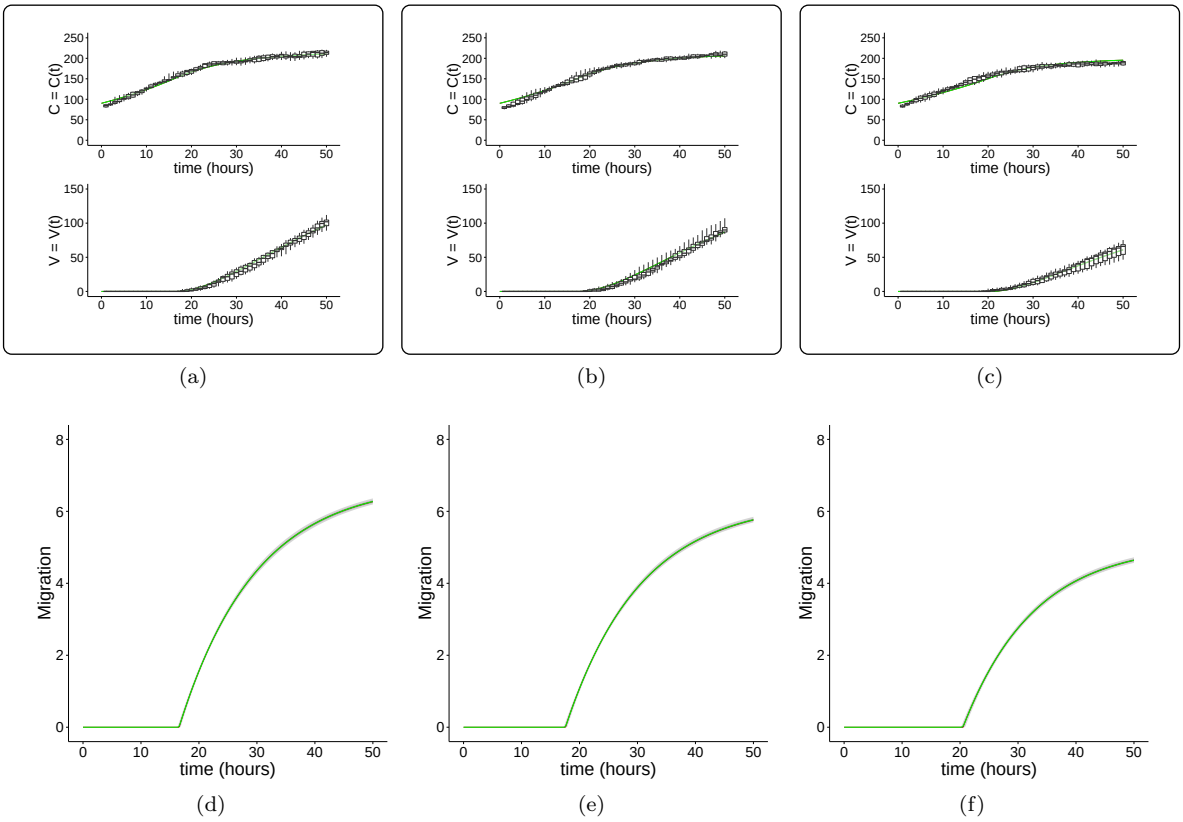

Figure 5: **Fits of the two-compartment model to simulated time course data**. (a)-(b)-(c) Posterior predictive distributions and estimates of parameter uncertainty obtained by fitting the two-compartment model (Eqs. (1)) against simulated time courses. Posterior predictive distributions inferred from (a) BrdU (control), (b) acute injury, (c) chronic injury experimental time courses. Boxplots represent the 0.05, 0.25, 0.75, 0.95 quantiles of the experimental data. Grey area plots represent the 0.05, 0.25, 0.75, 0.95 quantiles of the posterior predictive distributions (red line: posterior median; green line: posterior mean). (d)-(e)-(f) Plots representing the posterior predictive distribution of the migration term $\gamma(C - C^*)H(C - C^*)$ in simulated data obtained from simulated control (BrdU) (d), simulated acute injury (e) and simulated chronic injury (f) time courses. Contribution to migration is reduced during simulated chronic injury.

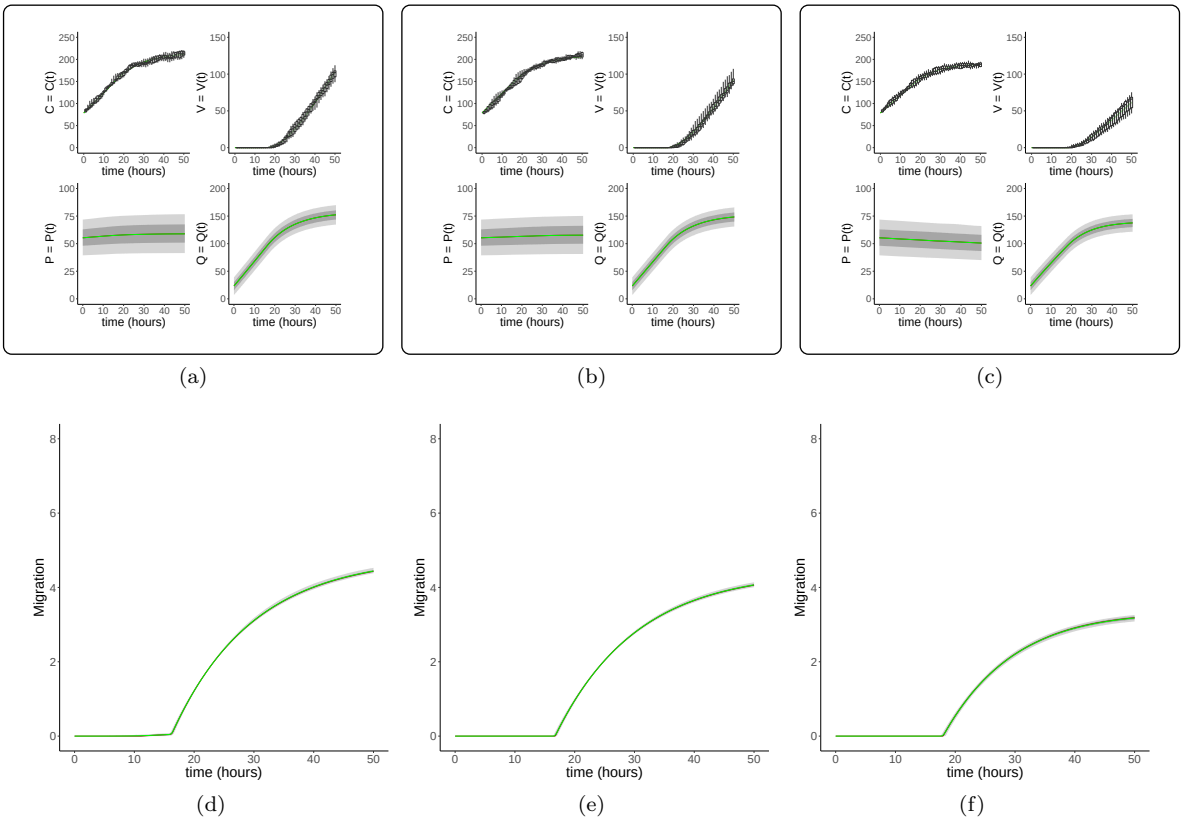

Figure 6: **Fits of the three-compartment model to simulated time course data**. (a)-(b)-(c) Posterior predictive distributions and estimates of parameter uncertainty obtained by fitting the three-compartment model (Eqs. (2)) against simulated time courses. Posterior predictive distributions inferred from (a) BrdU (control), (b) acute injury, (c) chronic injury experimental time courses. Boxplots represent the 0.05, 0.25, 0.75, 0.95 quantiles of the experimental data. Grey area plots represent the 0.05, 0.25, 0.75, 0.95 quantiles of the posterior predictive distributions (red line: posterior median; green line: posterior mean). (d)-(e)-(f) Plots representing the posterior predictive distribution of the migration term $\gamma_v(P-P^*)H(P-P^*)+\gamma_v(Q-Q^*)H(Q-Q^*)$ in simulated data obtained from simulated control (BrdU) (d), simulated acute injury (e) and simulated chronic injury (f) time courses. Contribution to migration is reduced during simulated chronic injury.

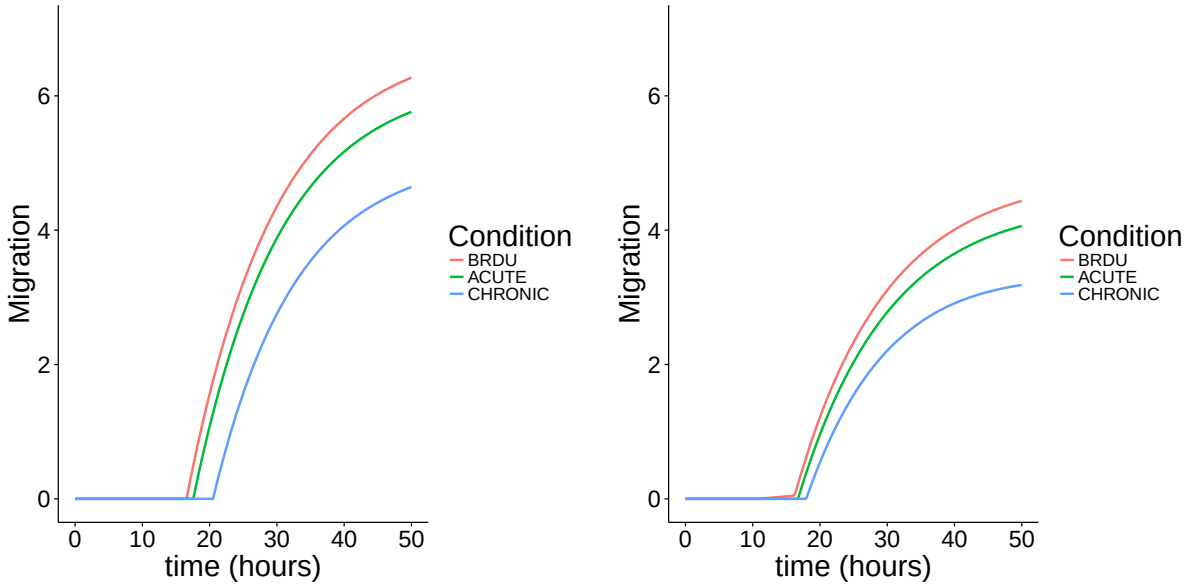

(a) (b)

Figure 7: **Simulated time courses, migration terms**. Plots representing the medians of the posterior predictive distribution of the migration terms obtained when fitting the two-compartment model (a) and the three-compartment model (b) against simulated time courses. Contribution to migration is reduced during simulated chronic injury.

Parameter posterior distributions

In this section we report the parameter posterior distributions, pairs plots and correlations derived from the posterior distribution when fitting the compartment models against experimental time courses by applying MCMC. Supplementary Figures 8 and 9 show the quantiles of the parameter posteriors of the two- and three-compartment models in ileum and duodenum. Supplementary Figures 10 and 11 show the quantiles of the parameter posteriors of the two- and three-compartment models when fitting simulated data. Supplementary Figures 12 - 15 show parameter pairs plots and marginal distributions obtained when fitting the two-compartment model against the ileal and duodenal time courses. Supplementary Figures 16 - 19 show parameter pairs plots and marginal distributions obtained when fitting the three-compartment model against the ileal and duodenal time courses. Supplementary Figures 20 - 23 show parameter pairs plots and marginal distributions obtained when fitting the two- and three-compartment models against the simulated time courses. The parameter σ_{fit} represents the inferred standard deviation.

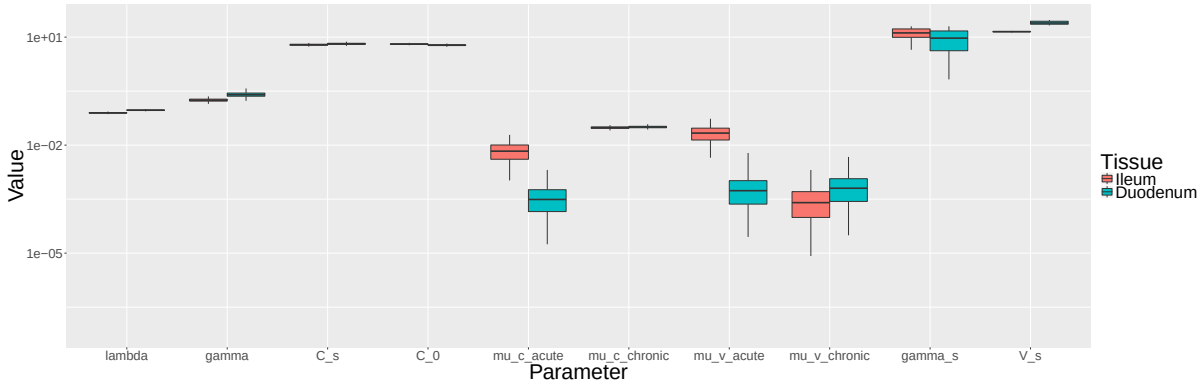

Figure 8: **Parameter posterior distributions of the two-compartment model (Eqs. (1)) in ileal and duodenal time courses**. Boxplots show the 0.05, 0.25, 0.75, 0.95 quantiles of the estimated parameters using the MCMC posterior draws.

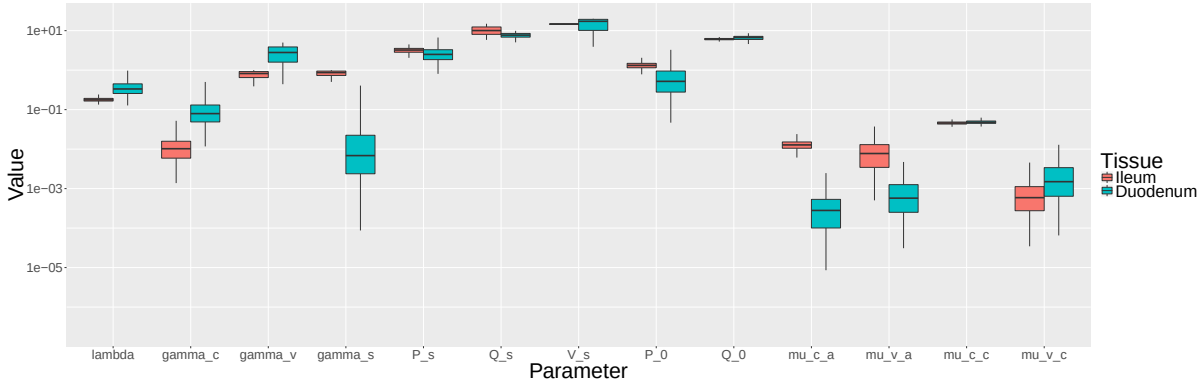

Figure 9: **Parameter posterior distributions of the three-compartment model (Eqs. (2)) in ileal and duodenal time courses**. Boxplots show the 0.05, 0.25, 0.75, 0.95 quantiles of the estimated parameters using the MCMC posterior draws.

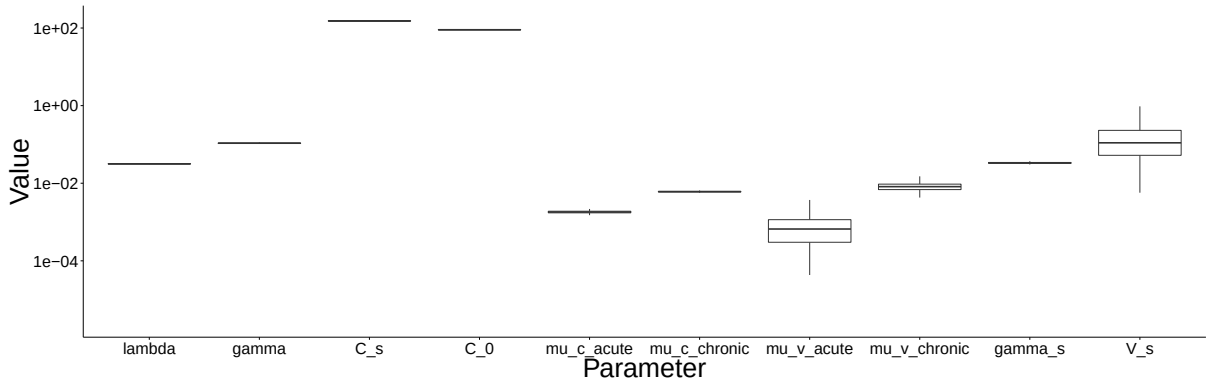

Figure 10: **Parameter posterior distributions of the two-compartment model (Eqs. (1)) in simulated time courses**. Boxplots show the 0.05, 0.25, 0.75, 0.95 quantiles of the estimated parameters using the MCMC posterior draws.

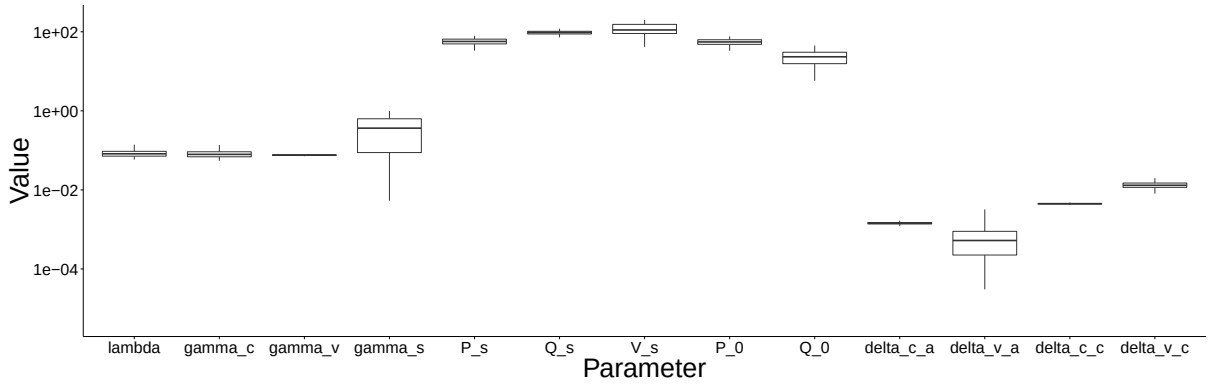

Figure 11: **Parameter posterior distributions of the three-compartment model (Eqs. (2)) in simulated time courses**. Boxplots show the 0.05, 0.25, 0.75, 0.95 quantiles of the estimated parameters using the MCMC posterior draws.

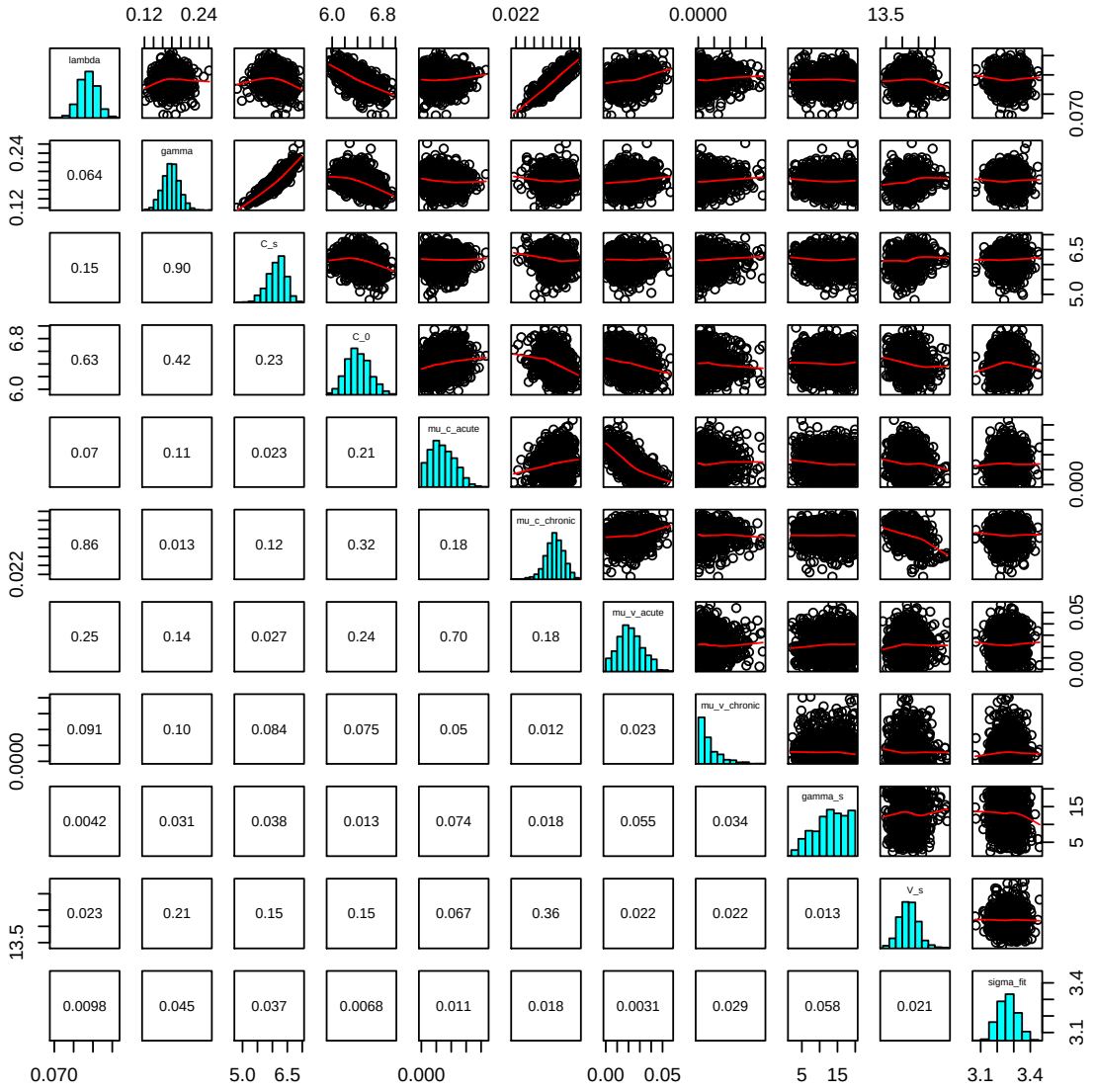

Figure 12: **Pairs plots of the posterior distribution of the two-compartment model (Eqs. (1)) in ileum**. This plot visualises the pairwise relationships in the upper panel, the correlation coefficients in the lower panel, and the marginal distribution for each parameter, represented by a histogram, on the diagonal.

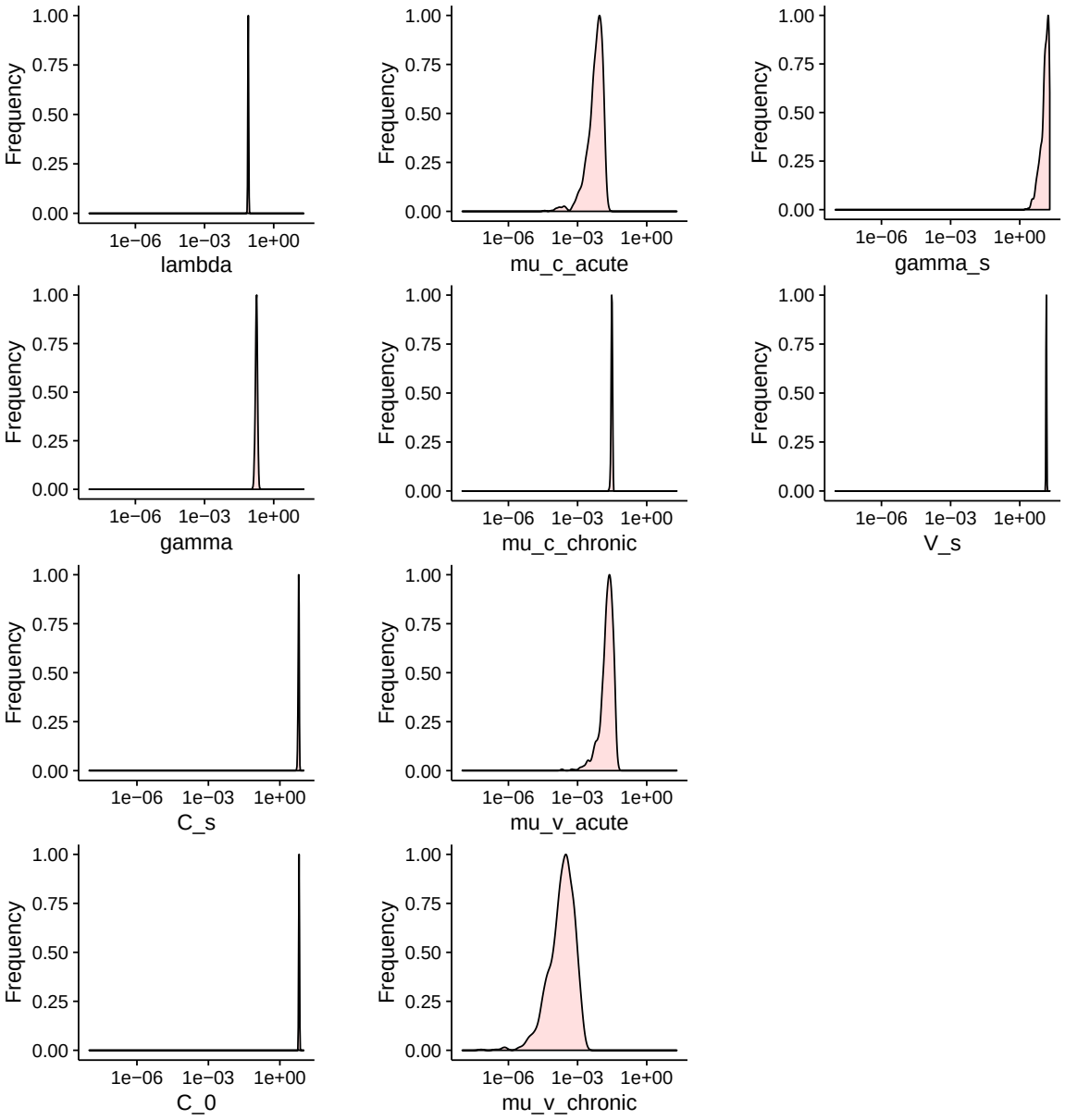

Figure 13: **Density plots of the posterior distribution of the two-compartment model (Eqs. (1)) in ileum**. This plot visualises the marginal distribution for each parameter as in the diagonal in Figure 12 but with upper boundaries in the parameter axis given by the parameter search space (uniform prior distribution). Because of the log-representation, the parameters are plotted with lower boundary in the horizontal axis given by the value 10^{-8} instead of 0 as in the parameter search space. The plot highlights how much the range of the parameter posterior is restricted compared to the prior.

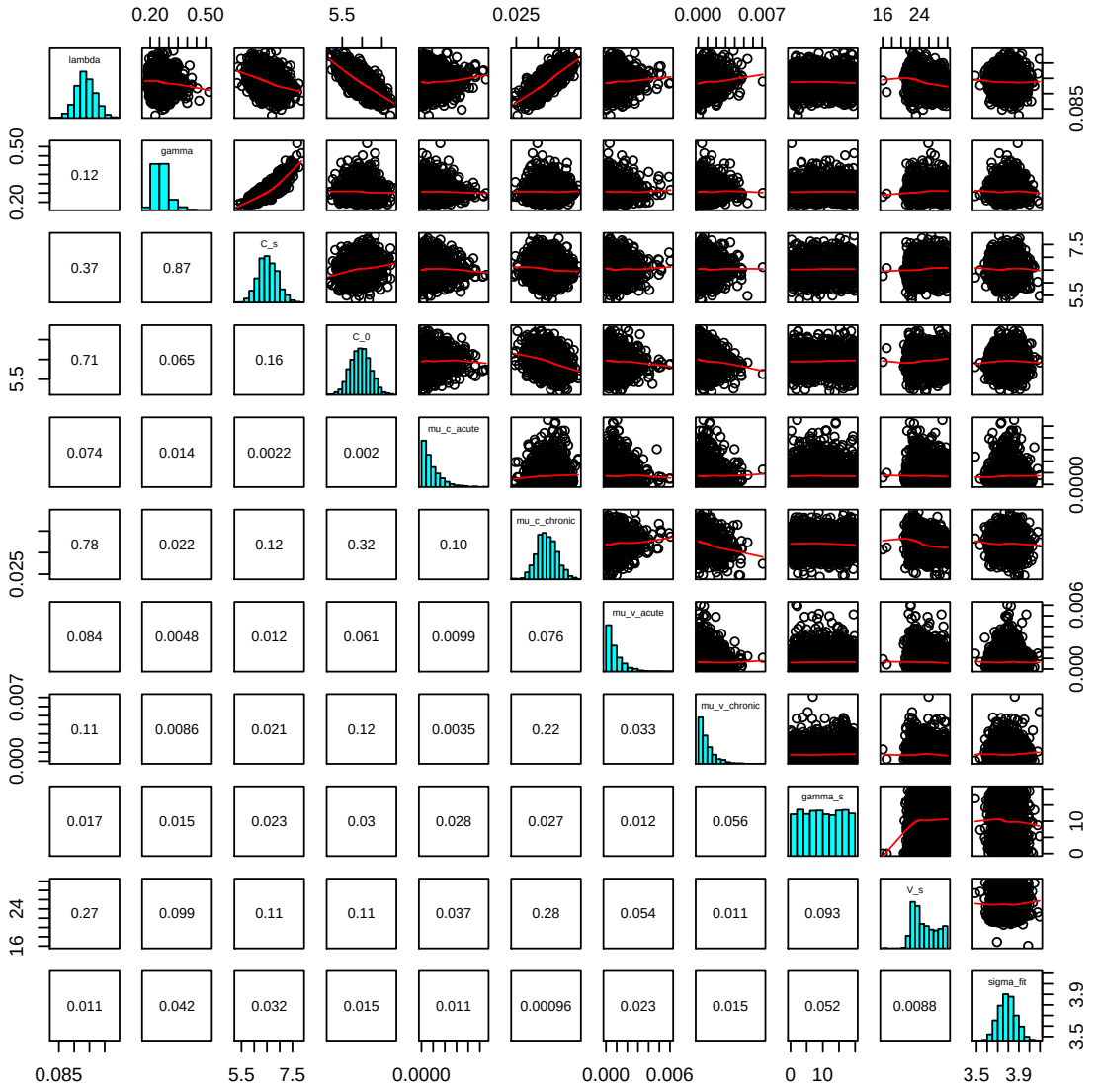

Figure 14: **Pairs plots of the posterior distribution of the two-compartment model (Eqs. (1)) in duodenum**. This plot visualises the pairwise relationships in the upper panel, the correlation coefficients in the lower panel, and the marginal distribution for each parameter, represented by a histogram, on the diagonal.

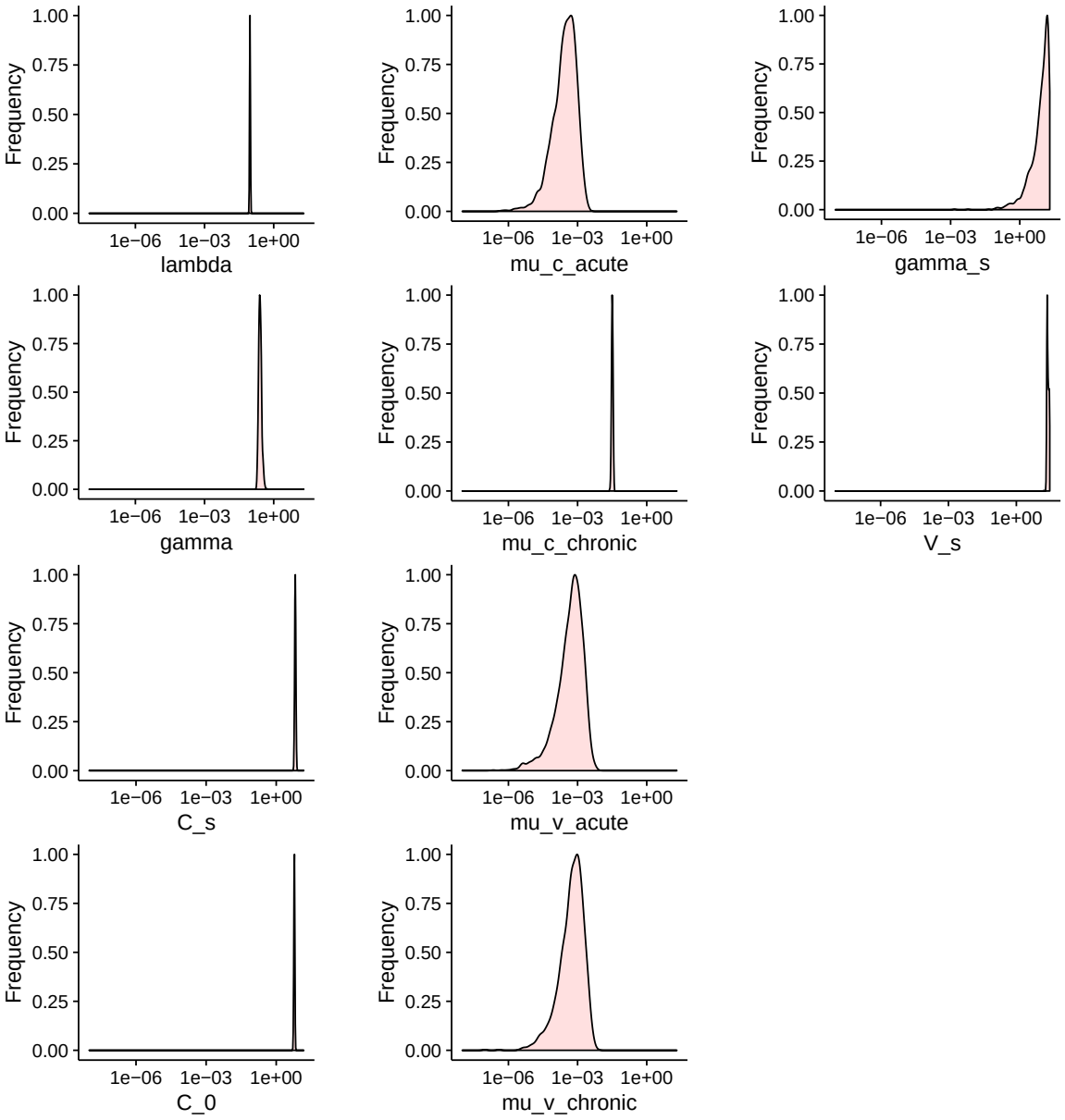

Figure 15: **Density plots of the posterior distribution of the two-compartment model (Eqs. (1)) in duodenum**. This plot visualises the marginal distribution for each parameter as in the diagonal in Figure 14 but with upper boundaries in the parameter axis given by the parameter search space (uniform prior distribution). Because of the log-representation, the parameters are plotted with lower boundary in the horizontal axis given by the value 10^{-8} instead of 0 as in the parameter search space. The plot highlights how much the range of the parameter posterior is restricted compared to the prior.

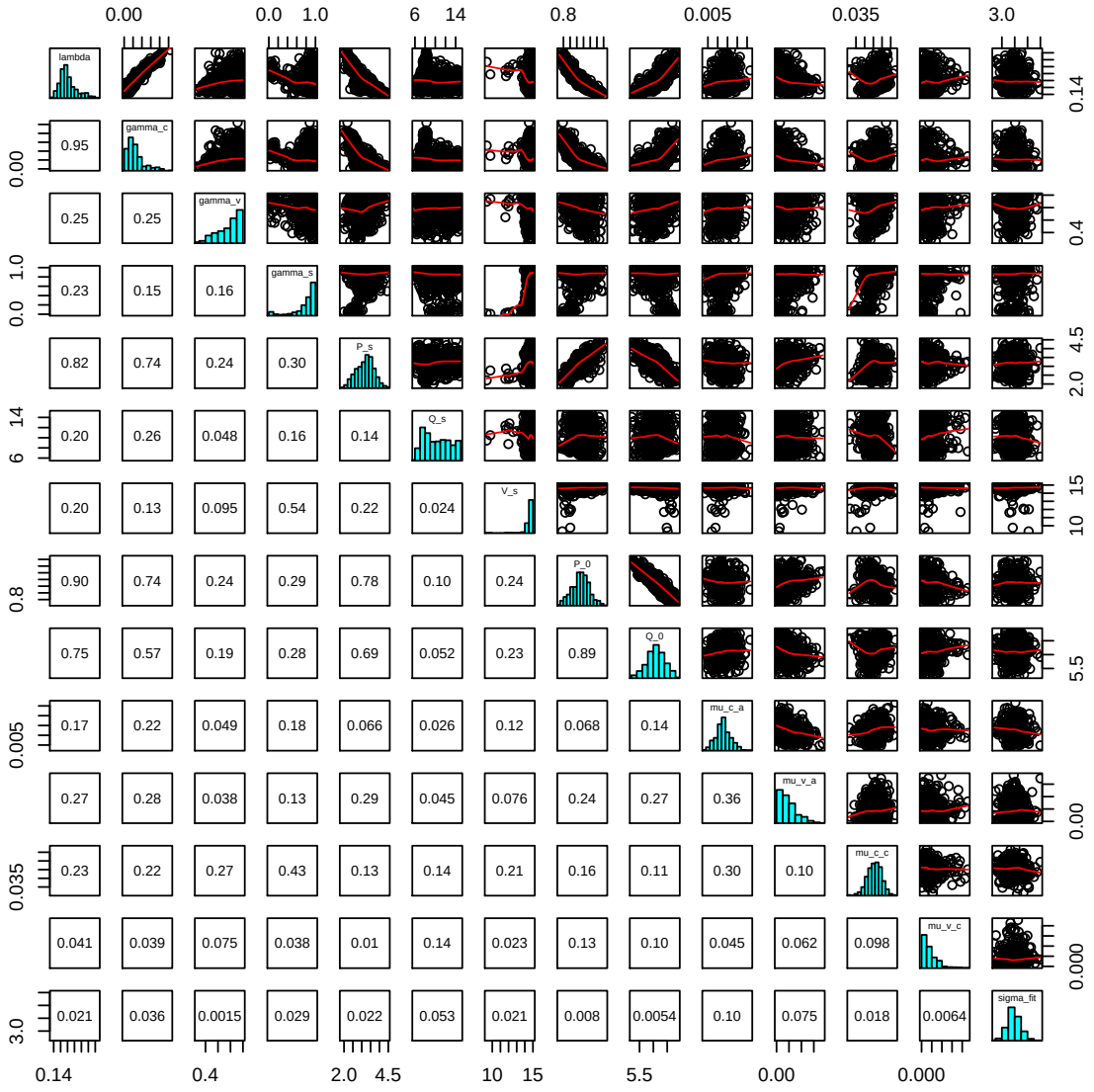

Figure 16: **Pairs plots of the posterior distribution of the three-compartment model (Eqs. (2)) in ileum**. This plot visualises the pairwise relationships in the upper panel, the correlation coefficients in the lower panel, and the marginal distribution for each parameter, represented by a histogram, on the diagonal.

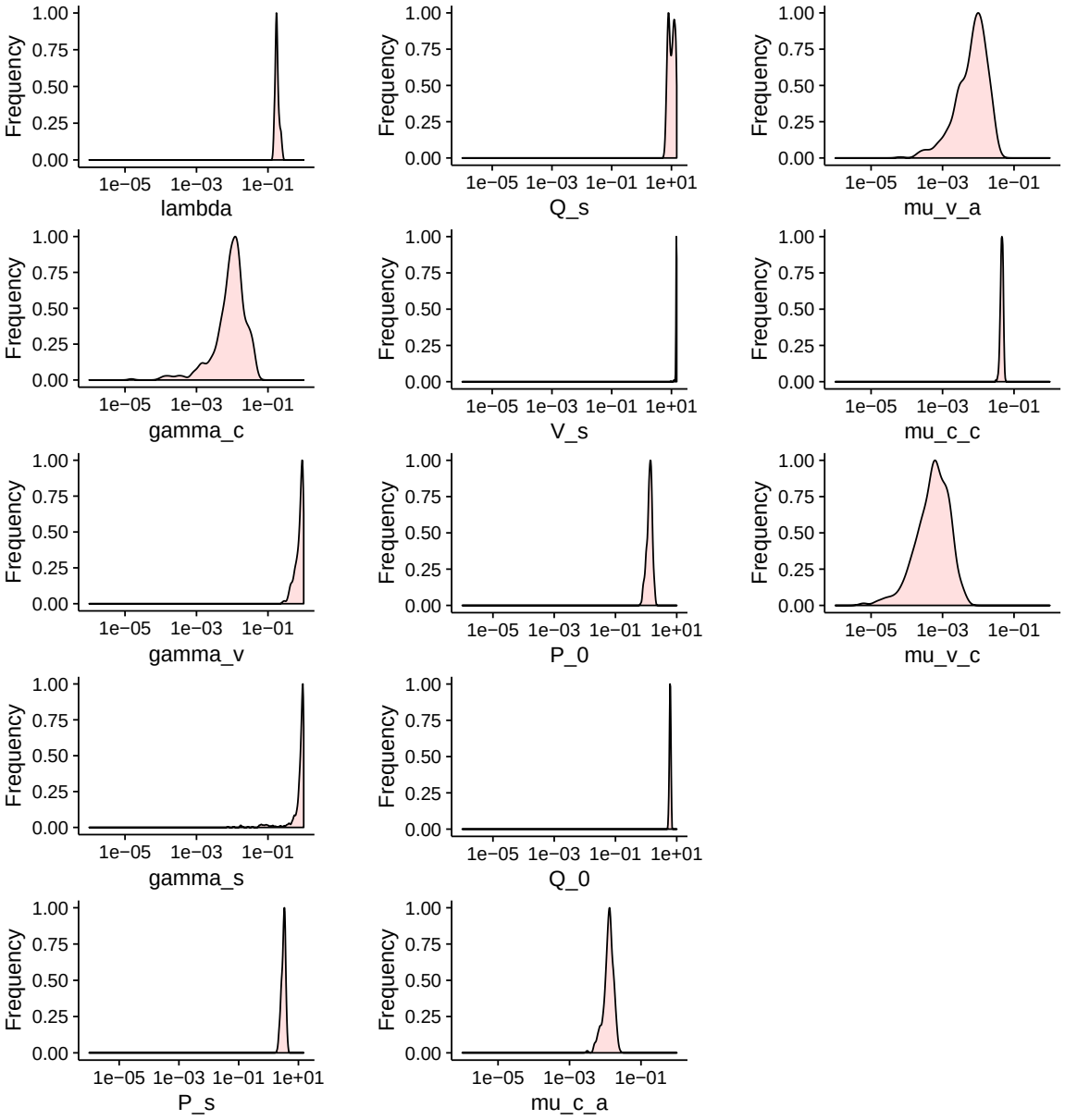

Figure 17: **Density plots of the posterior distribution of the three-compartment model (Eqs. (2)) in ileum**. This plot visualises the marginal distribution for each parameter as in the diagonal in Figure 16 but with upper boundaries in the parameter axis given by the parameter search space (uniform prior distribution). Because of the log-representation, the parameters are plotted with lower boundary in the horizontal axis given by the value 10^{-6} instead of 0 as in the parameter search space. The plot highlights how much the range of the parameter posterior is restricted compared to the prior.

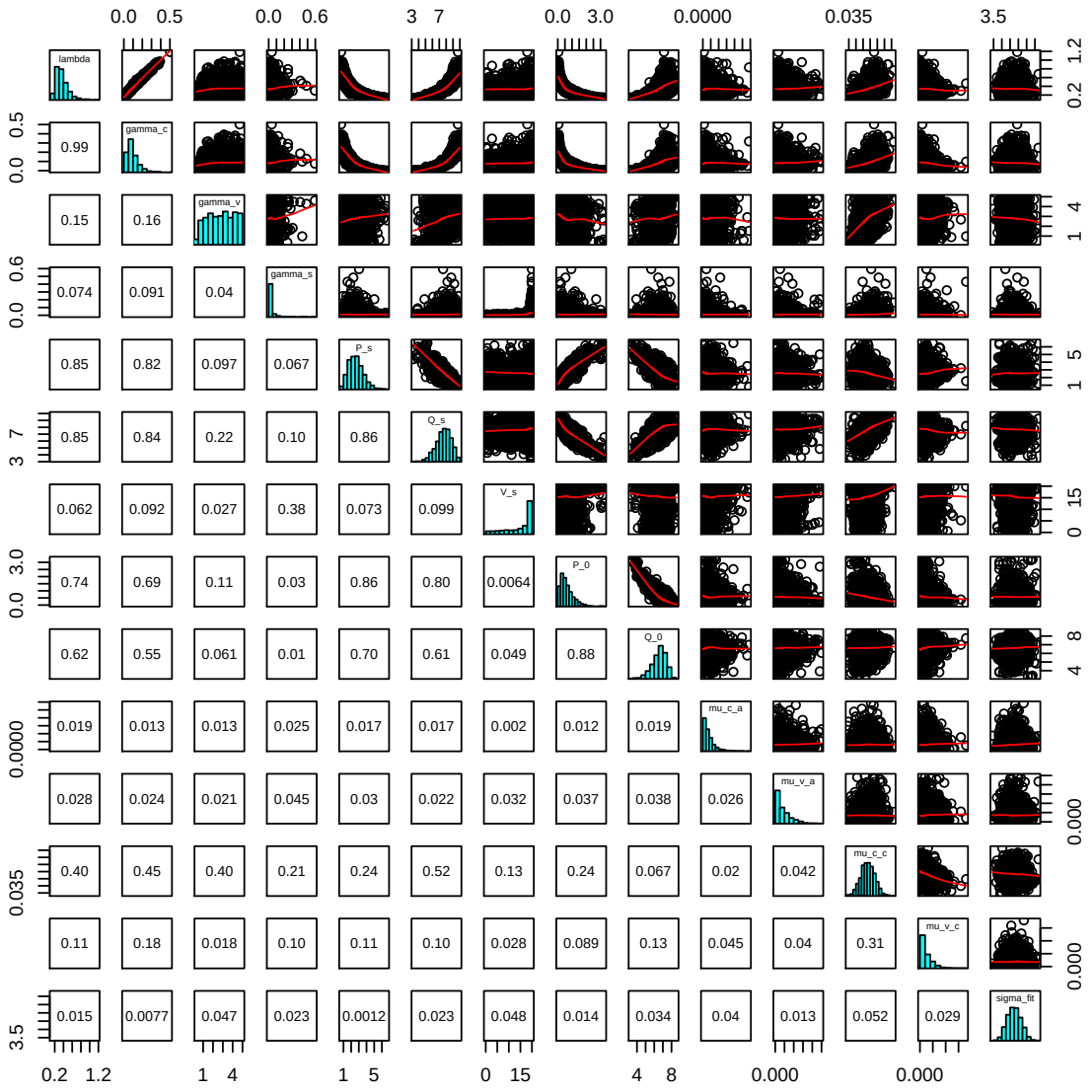

Figure 18: **Pairs plots of the posterior distribution of the three-compartment model (Eqs. (2)) in duodenum**. This plot visualises the pairwise relationships in the upper panel, the correlation coefficients in the lower panel, and the marginal distribution for each parameter, represented by a histogram, on the diagonal.

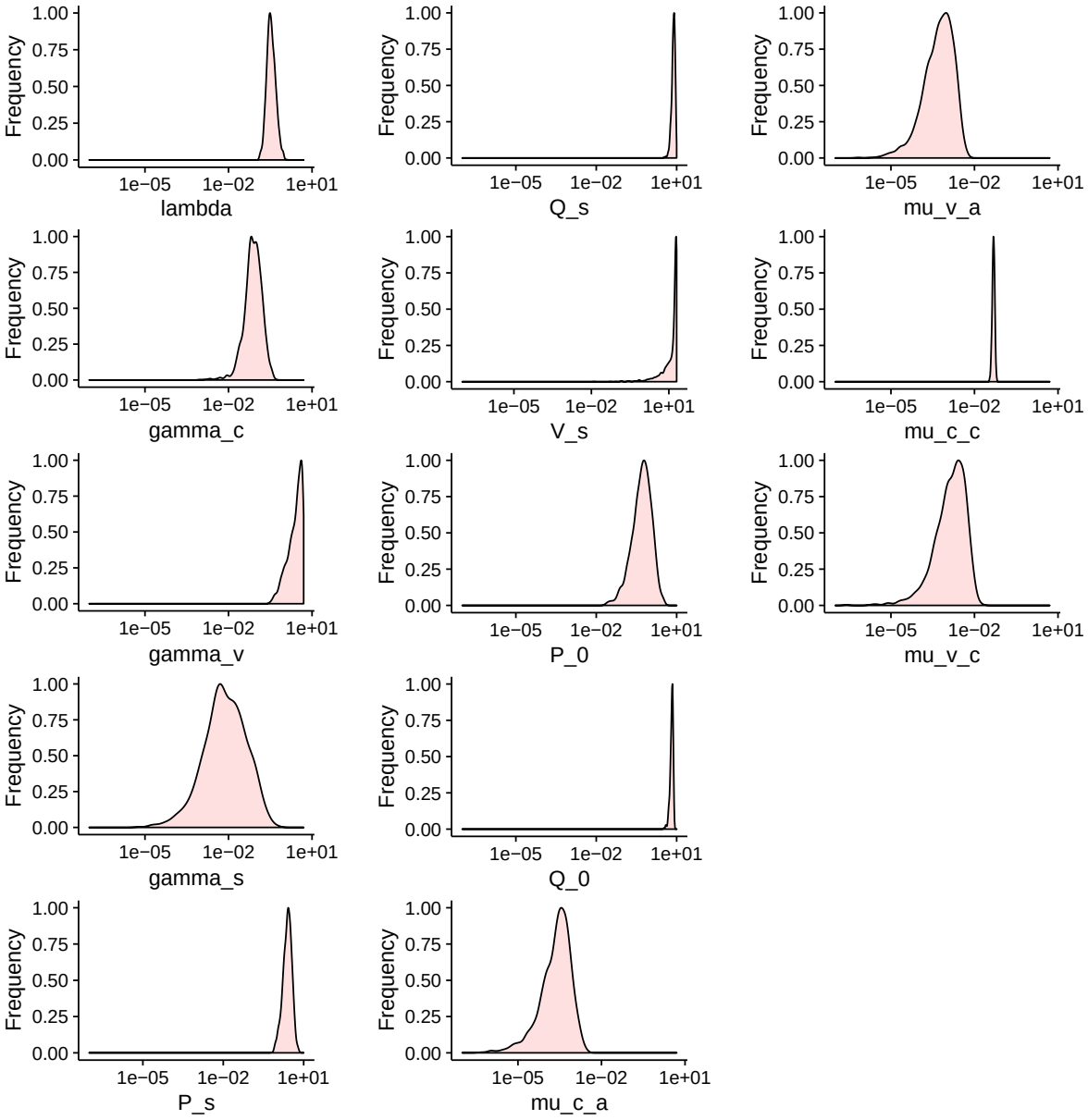

Figure 19: **Density plots of the posterior distribution of the three-compartment model (Eqs. (2)) in duodenum**. This plot visualises the marginal distribution for each parameter as in the diagonal in Figure 18 but with upper boundaries in the parameter axis given by the parameter search space (uniform prior distribution). Because of the log-representation, the parameters are plotted with lower boundary in the horizontal axis given by the value 10^{-7} instead of 0 as in the parameter search space. The plot highlights how much the range of the parameter posterior is restricted compared to the prior.

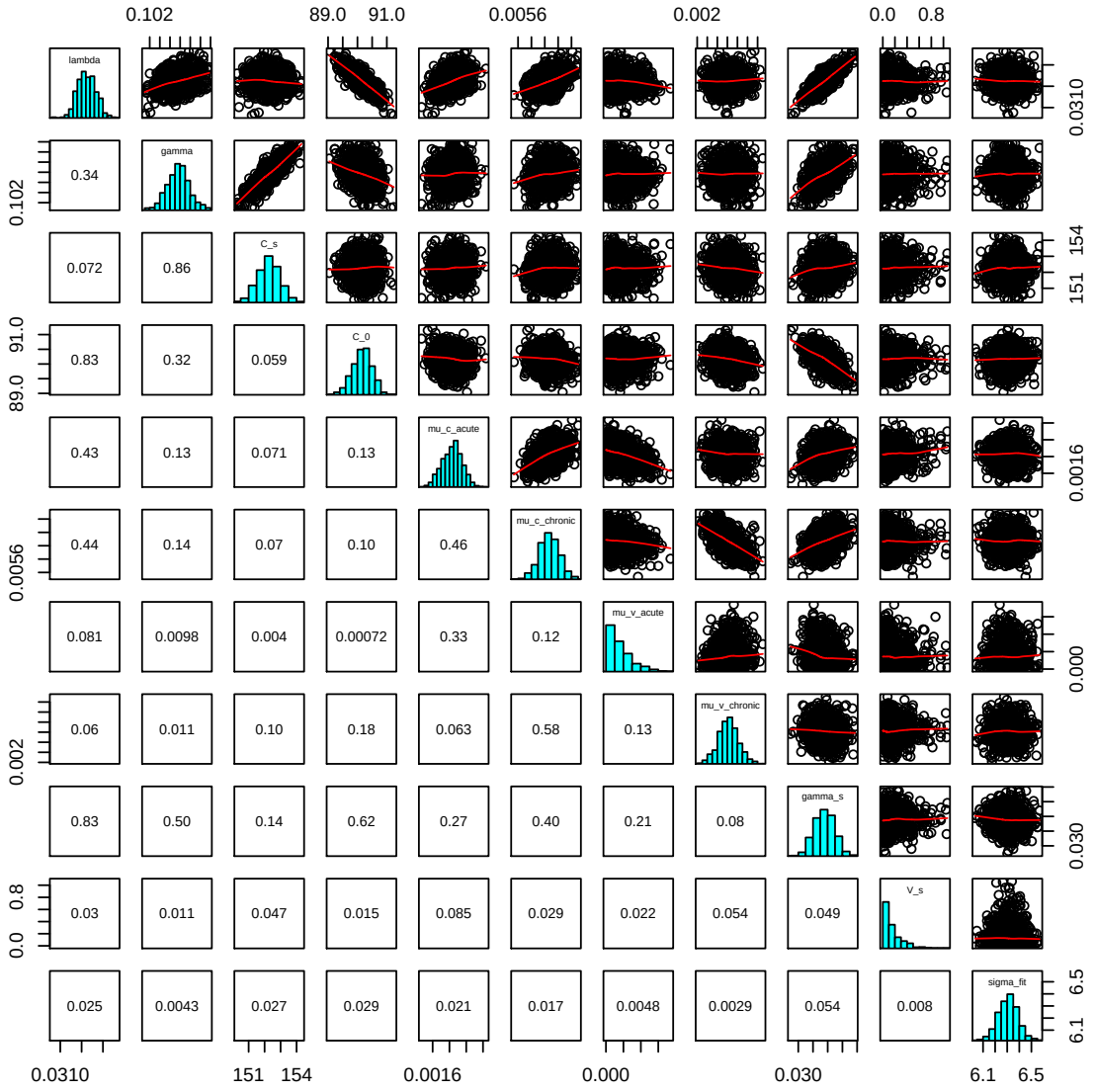

Figure 20: **Pairs plots of the posterior distribution of the two-compartment model (Eqs. (1)) fitted against simulated data**. This plot visualises the pairwise relationships in the upper panel, the correlation coefficients in the lower panel, and the marginal distribution for each parameter, represented by a histogram, on the diagonal.

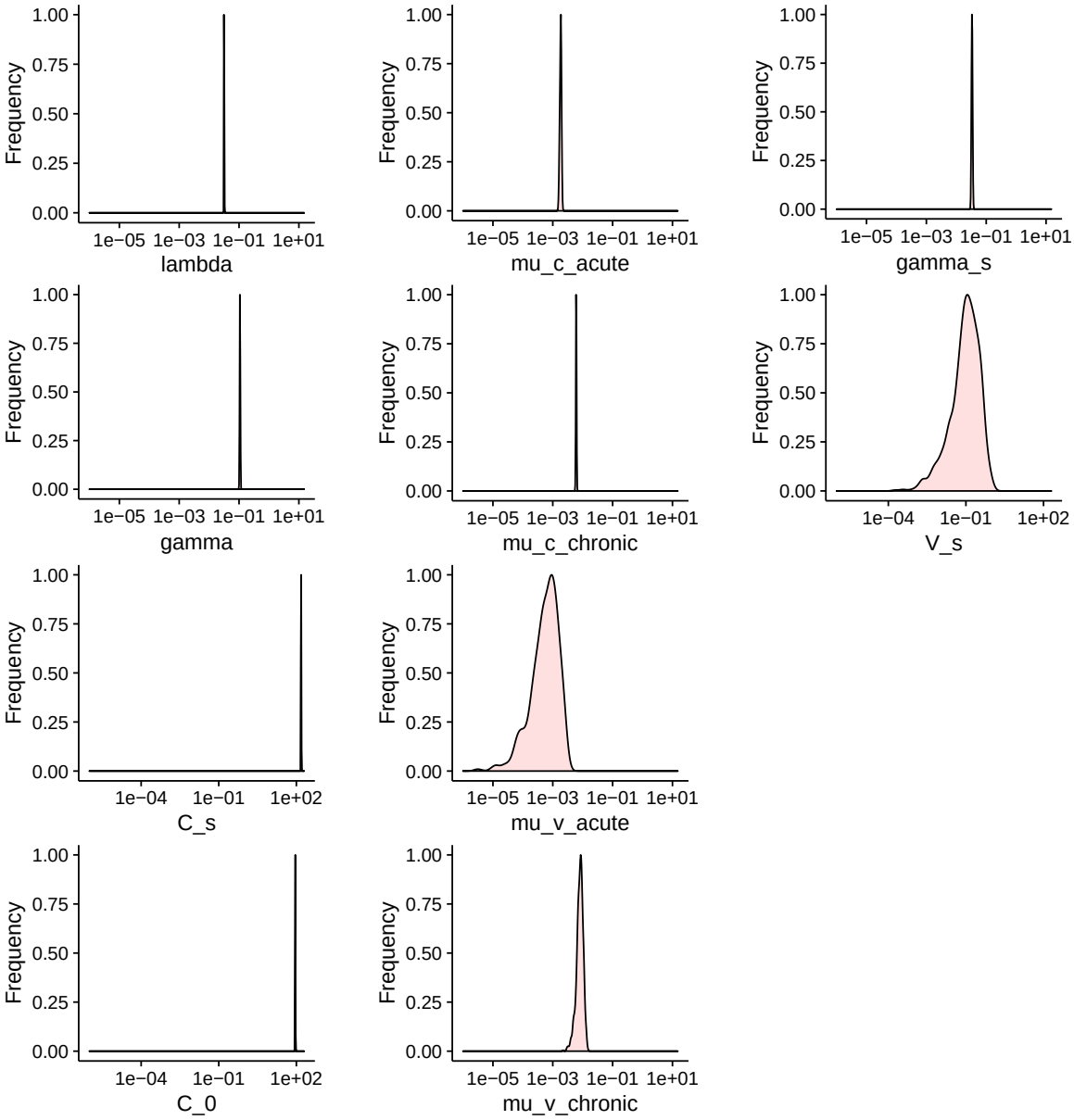

Figure 21: **Density plots of the posterior distribution of the two-compartment model (Eqs. (1)) fitted against simulated data**. This plot visualises the marginal distribution for each parameter as in the diagonal in Figure 20 but with upper boundaries in the parameter axis given by the parameter search space (uniform prior distribution). Because of the log-representation, the parameters are plotted with lower boundary in the horizontal axis given by the value 10^{-6} instead of 0 as in the parameter search space. The plot highlights how much the range of the parameter posterior is restricted compared to the prior.

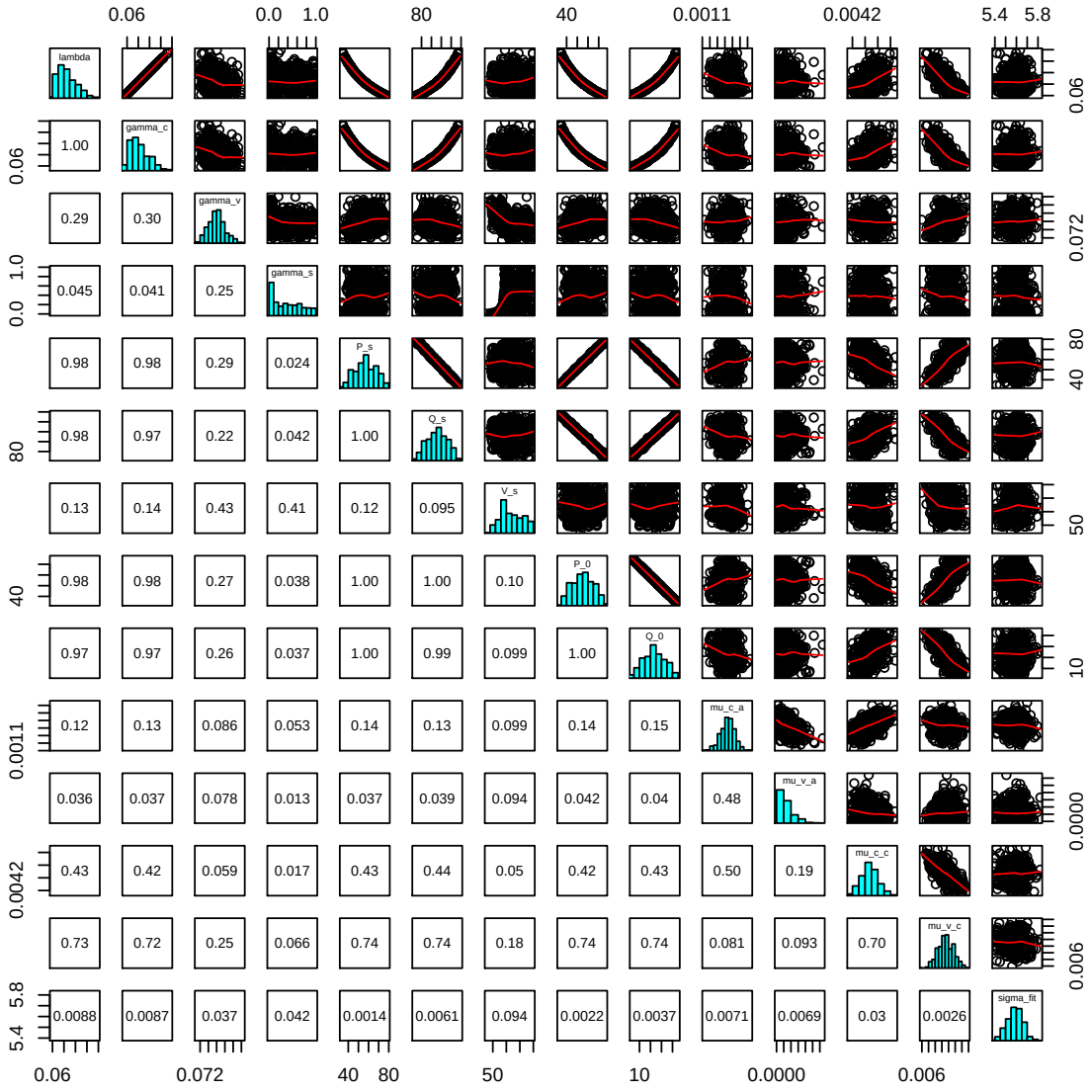

Figure 22: **Pairs plots of the posterior distribution of the three-compartment model (Eqs. (2)) fitted against simulated data**. This plot visualises the pairwise relationships in the upper panel, the correlation coefficients in the lower panel, and the marginal distribution for each parameter, represented by a histogram, on the diagonal.

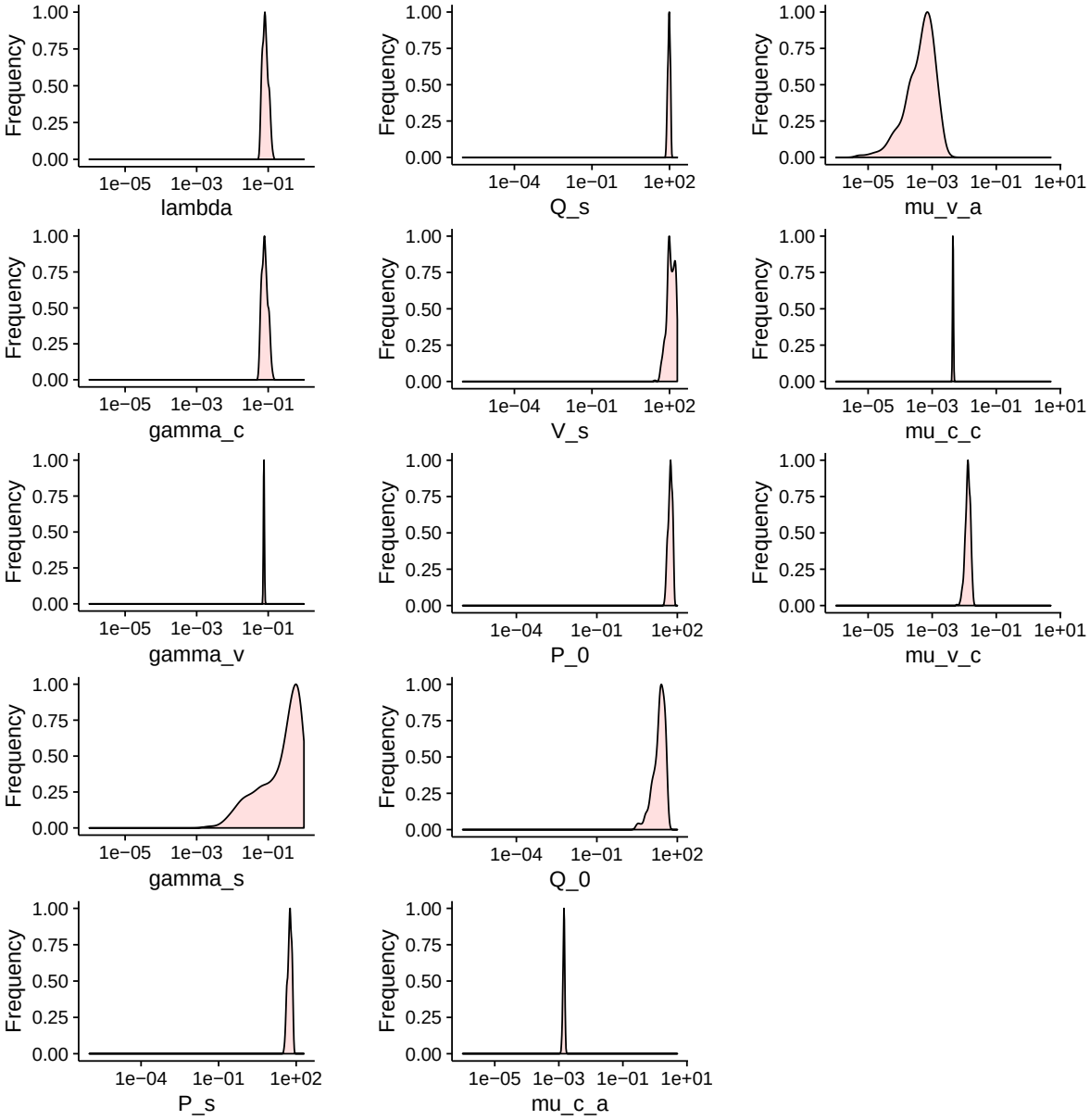

Figure 23: **Density plots of the posterior distribution of the three-compartment model (Eqs. (2)) fitted against simulated data**. This plot visualises the marginal distribution for each parameter as in the diagonal in Figure 22 but with upper boundaries in the parameter axis given by the parameter search space (uniform prior distribution). Because of the log-representation, the parameters are plotted with lower boundary in the horizontal axis given by the value 10^{-6} instead of 0 as in the parameter search space. The plot highlights how much the range of the parameter posterior is restricted compared to the prior.

Qualitative dynamics of the two-compartment model

In what follows, we analyse the qualitative dynamics of the two-compartment model:

$$\frac{dC}{dt} = \phi C - \gamma(C - C^*)H(C - C^*)$$
$$\frac{dV}{dt} = \gamma(C - C^*)H(C - C^*) - \mu_v V - \gamma_s(V - V^*)H(V - V^*), \quad (1)$$

with $\phi = \lambda - \mu_c$. We define by t_C^* and t_V^* the time thresholds after which $C(t) > C^*$ and $V(t) > V^*$, respectively. Supplementary Figure 24 presents typical simulation results obtained when perturbing the parameters μ_c and μ_v which are specific to the conditions of acute and chronic injury. An increase in μ_c causes a delay of both time thresholds, whereas an increase in μ_v of t_V^* only. Supplementary Figures 25 - 27 show how the time thresholds vary when varying the model parameters and highlight that the parameters influencing both the time thresholds the most are λ, μ_c and C_0. In the simulations that follow, the model parameters are perturbed from the default values: $\lambda = 0.2\ h^{-1}$, $\gamma = 0.2\ h^{-1}$, $C_s = 8.0$, $C_0 = 4.0$, $\mu_c = 0.1\ h^{-1}$, $\mu_v = 0.1\ h^{-1}$, $\gamma_s = 0.001\ h^{-1}$, $V_s = 10.0$, $V_0 = 0.0$.

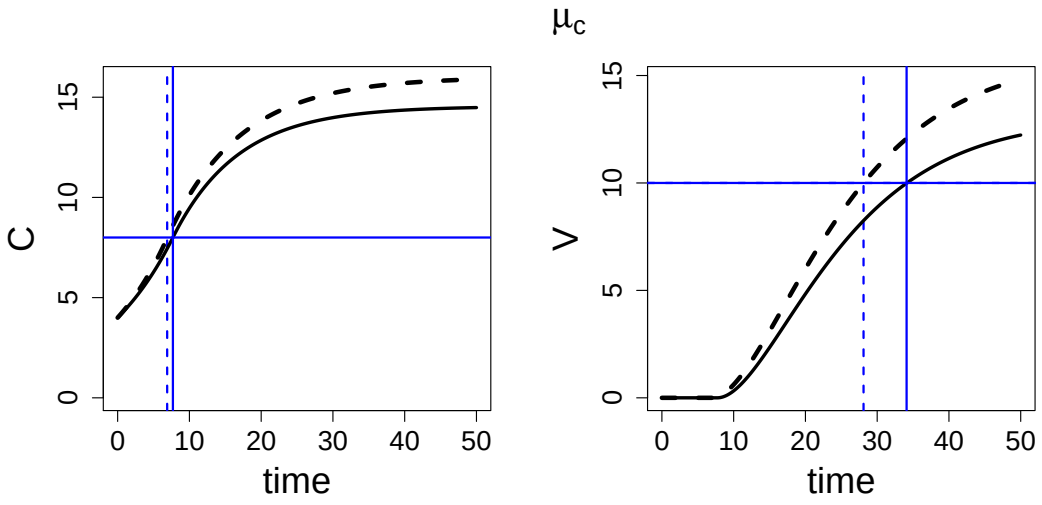

(a)

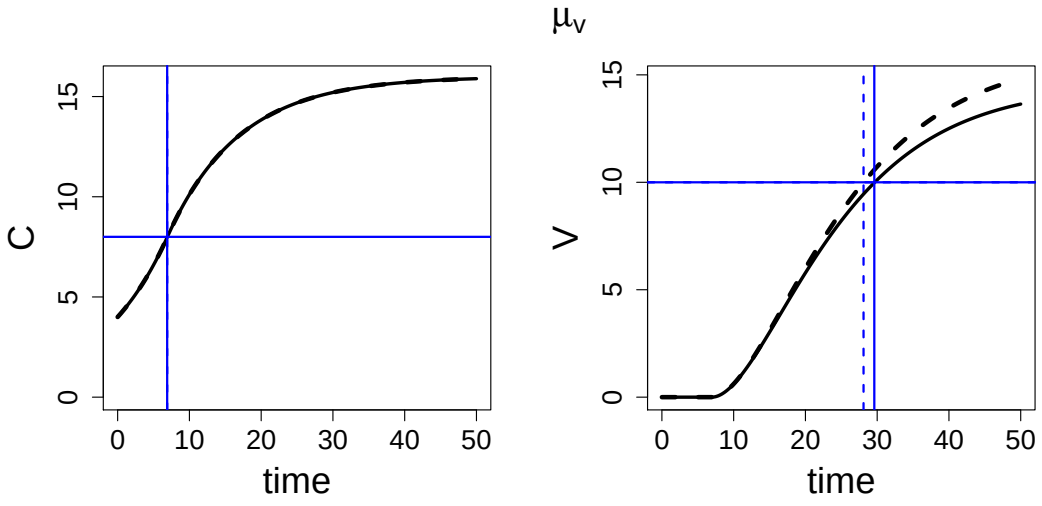

(b)

Figure 24: **Simulation of the two-compartment model when increasing μ_c (a) and μ_v (b)**. Dashed lines: model simulations (Eqs. (1) of the Main Text) with default parameter values. Solid lines: model simulations obtained when increasing the values of μ_c (a) and μ_v (b) of 10% from their default value. Black lines indicate simulated values of $C(t)$ and $V(t)$. Vertical blue lines indicate the time thresholds t_C^* and t_V^* after which migration and cell shedding occur. The horizontal blue lines indicate the thresholds C^* and V^*.

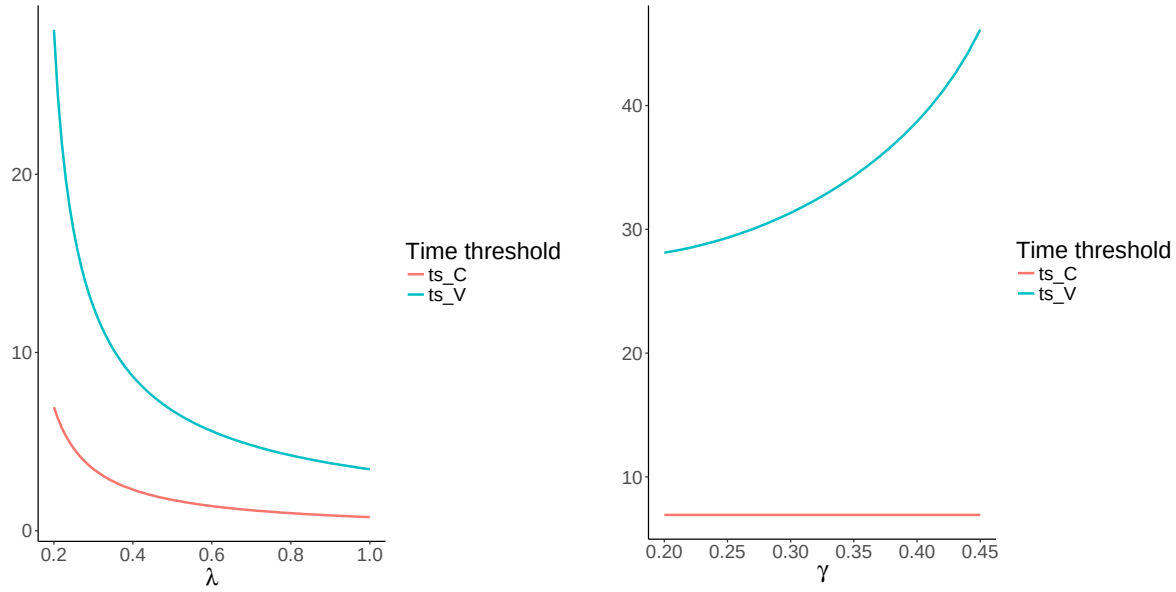

(a) (b)

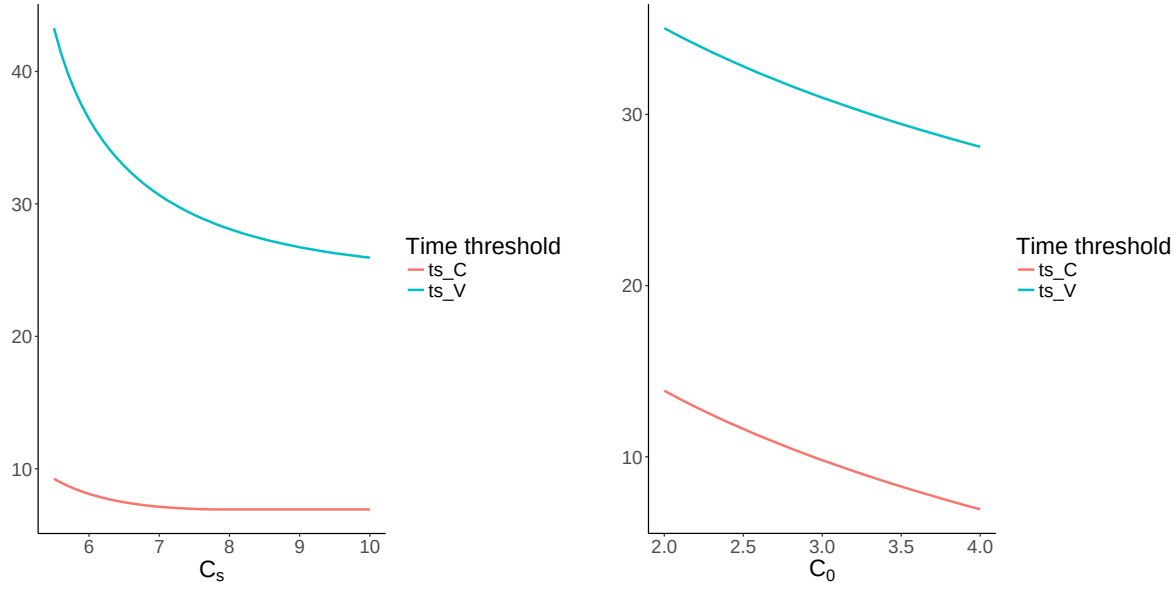

(c) (d)

Figure 25: **Time thresholds against parameters in the two-compartment model (1/3).**

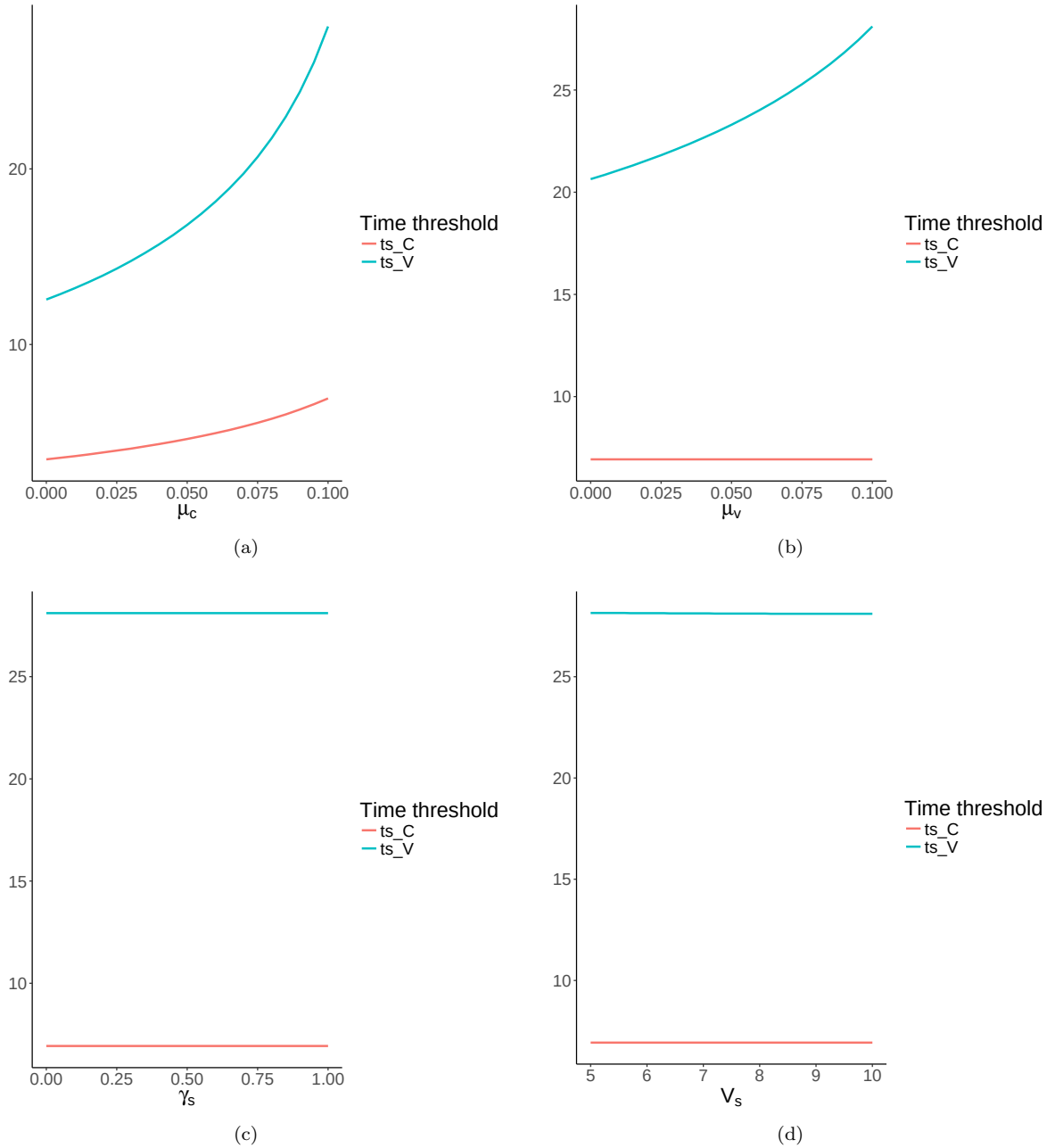

Figure 26: **Time thresholds against parameters in the two-compartment model (2/3).**

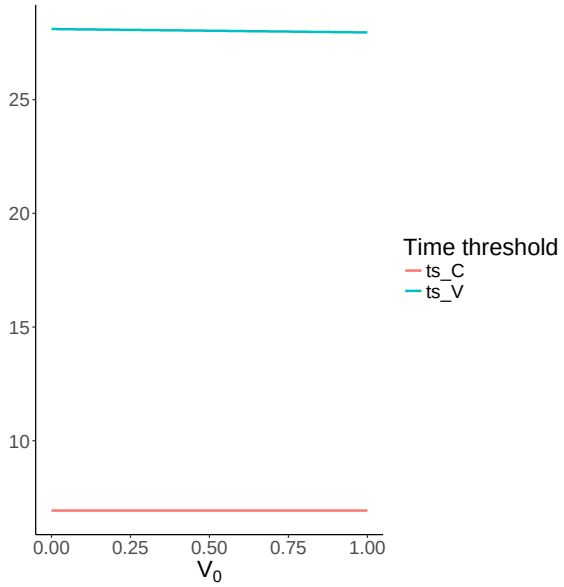

Figure 27: **Time thresholds against parameters in the two-compartment model (3/3)**.

Qualitative dynamics of the three-compartment model

In what follows, we analyse the qualitative dynamics of the three-compartment model:

$$\begin{aligned}
\frac{dP}{dt} &= \phi P - \gamma_v (P - P^*) H(P - P^*) \\
\frac{dQ}{dt} &= \gamma_c P - \mu_c Q - \gamma_v (Q - Q^*) H(Q - Q^*) \\
\frac{dV}{dt} &= \gamma_v (P - P^*) H(P - P^*) + \gamma_v (Q - Q^*) H(Q - Q^*) - \mu_v V - \gamma_s (V - V^*) H(V - V^*),
\end{aligned} \tag{2}$$

with $\phi = \lambda - \gamma_c - \mu_c$. We define by t_P^*, t_Q^*, t_C^* and t_V^* the time thresholds after which $P(t) > P^*$, $Q(t) > Q^*$, $C(t) := P(t) + Q(t) > P^* + Q^* := C^*$ and $V(t) > V^*$, respectively. Supplementary Figure 28 presents typical simulation results obtained when perturbing the parameters μ_c and μ_v which are specific to the conditions of acute and chronic injury. An increase in μ_c causes a delay of all time thresholds, whereas an increase in μ_v of t_V^* only. Supplementary Figures 29 - 31 show how the time thresholds vary when varying the model parameters and highlight that the parameters influencing all of the time thresholds the most are λ, γ_c, μ_c and P_0. In the simulations that follow, the model parameters are perturbed from the default values: $\lambda = 0.25\ h^{-1}$, $\gamma_c = 0.1\ h^{-1}$, $\gamma_v = 0.1\ h^{-1}$, $\mu_c = 0.1\ h^{-1}$, $\mu_v = 0.2\ h^{-1}$, $\gamma_s = 0.01\ h^{-1}$, $P_s = 10.0$, $P_0 = 5.0$, $Q_s = 5.0$, $Q_0 = 0.0$, $V_s = 4.0$, $V_0 = 0.0$.

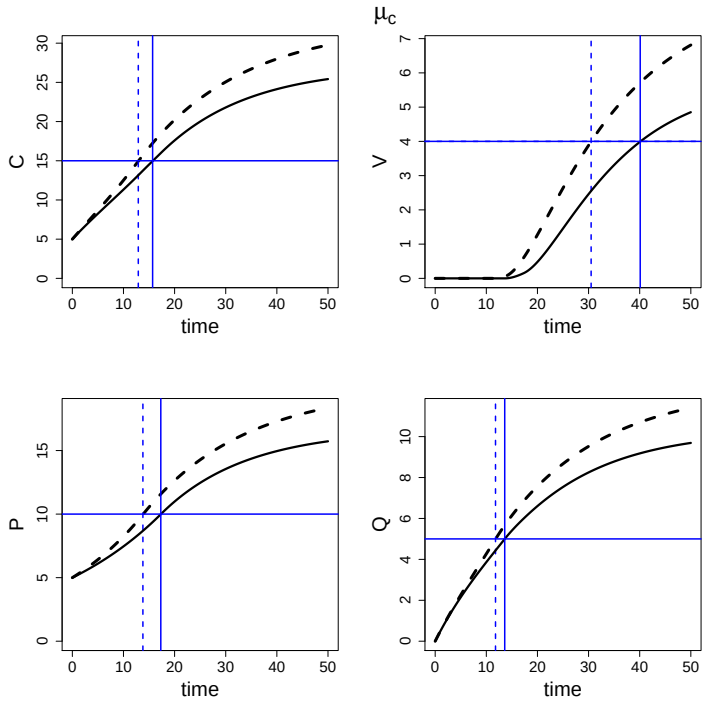

(a)

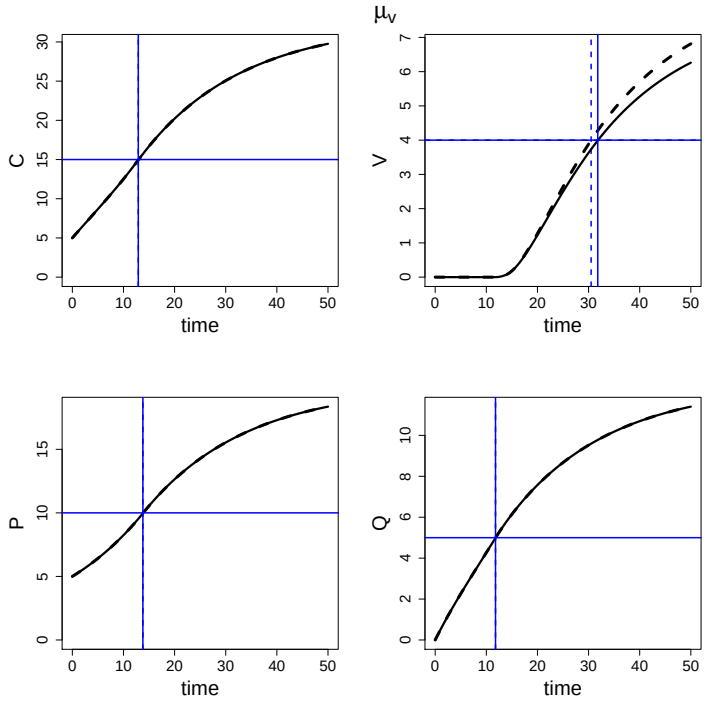

(b)

Figure 28: **Simulation of the three-compartment model when increasing μ_c (a) and μ_v (b)**. Dashed lines: model simulations (Eqs. (2) of the Main Text) with default parameter values. Solid lines: model simulations obtained when increasing the values of μ_c (a) and μ_v (b) of 10% from their default value. Black lines indicate simulated values of $P(t)$, $Q(t)$, $C(t)$ and $V(t)$. Vertical blue lines indicate the time thresholds t_P^*, t_Q^*, t_C^* and t_V^* after which migration and cell shedding occur. The horizontal blue lines indicate the thresholds P^*, Q^*, C^* and V^*.

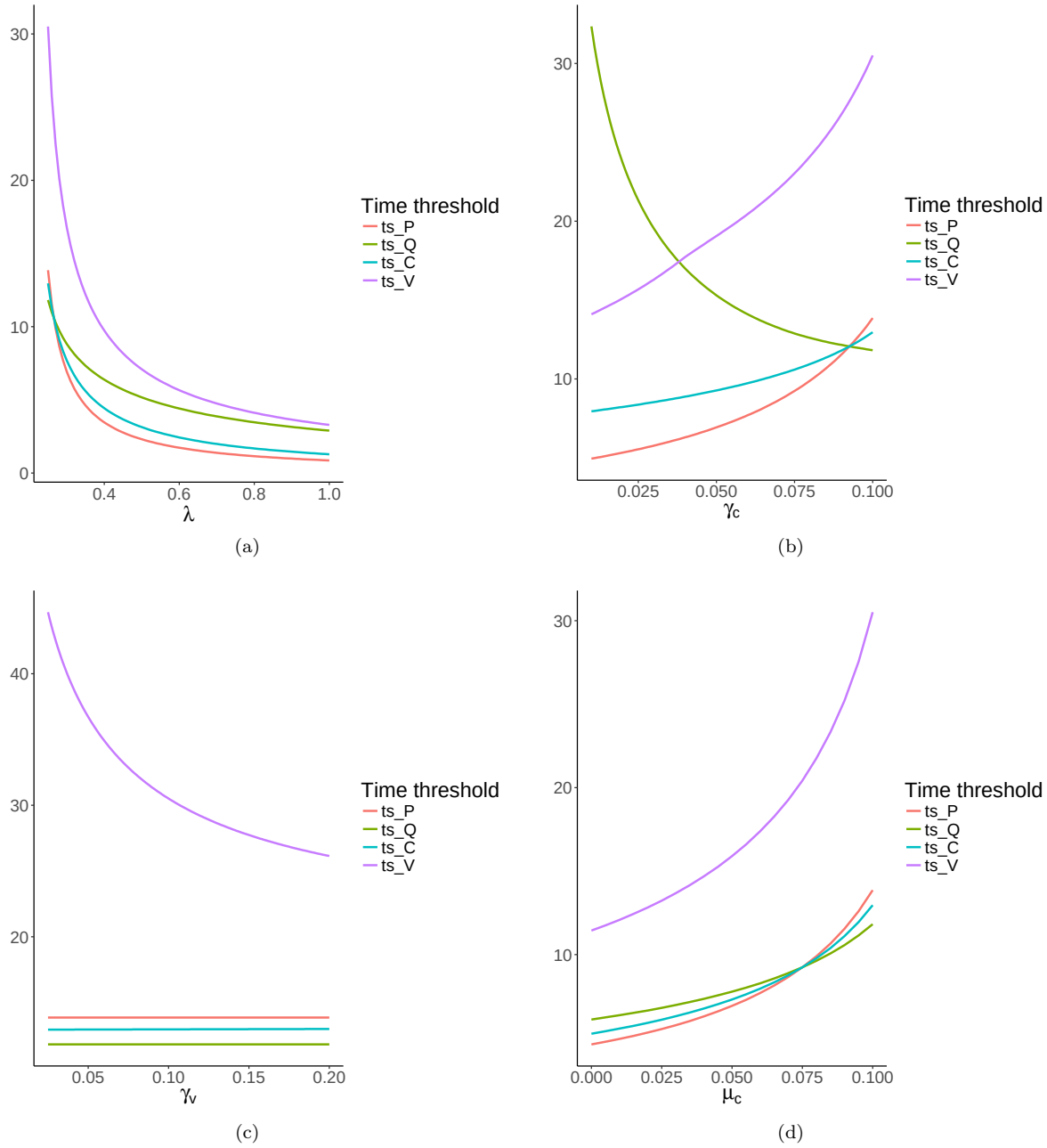

Figure 29: **Time thresholds against parameters in the three-compartment model (1/3).**

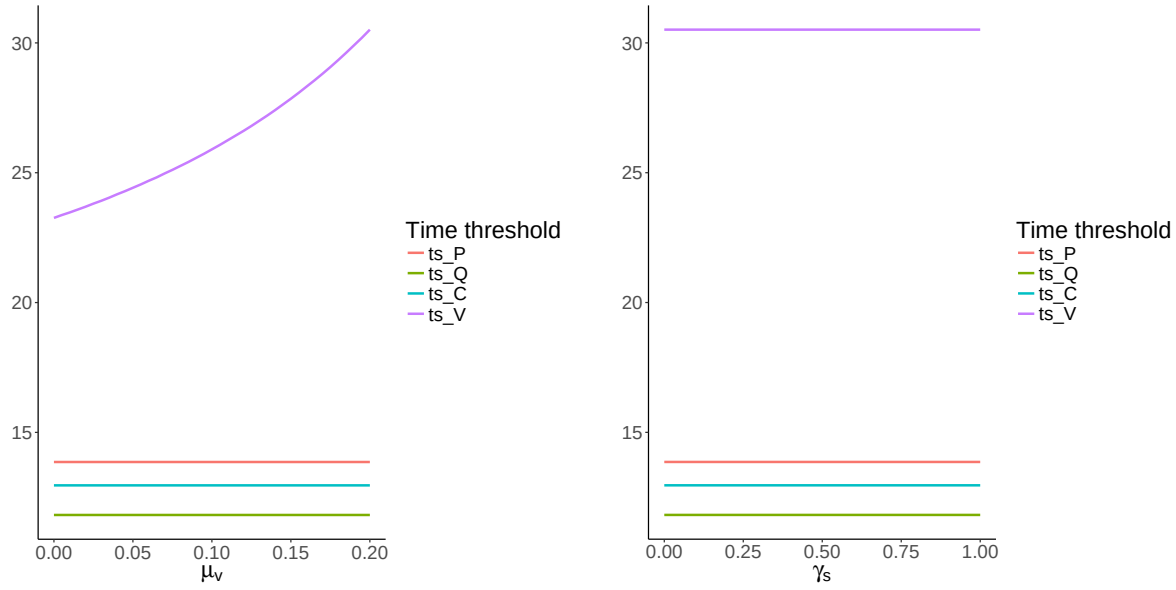

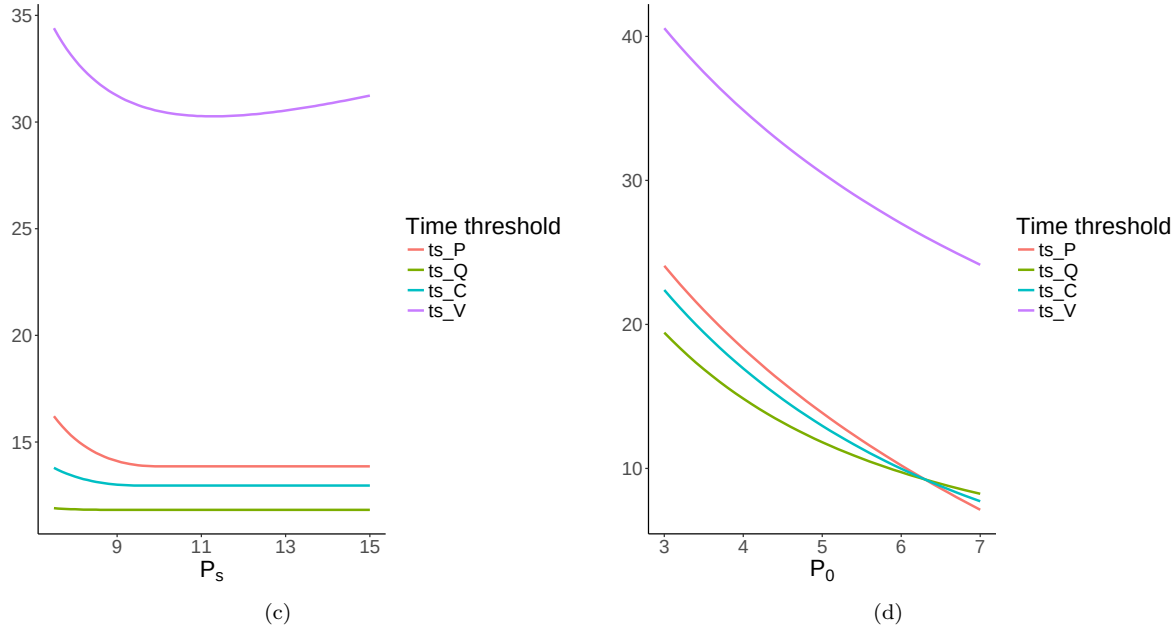

Figure 30: **Time thresholds against parameters in the three-compartment model (2/3).**

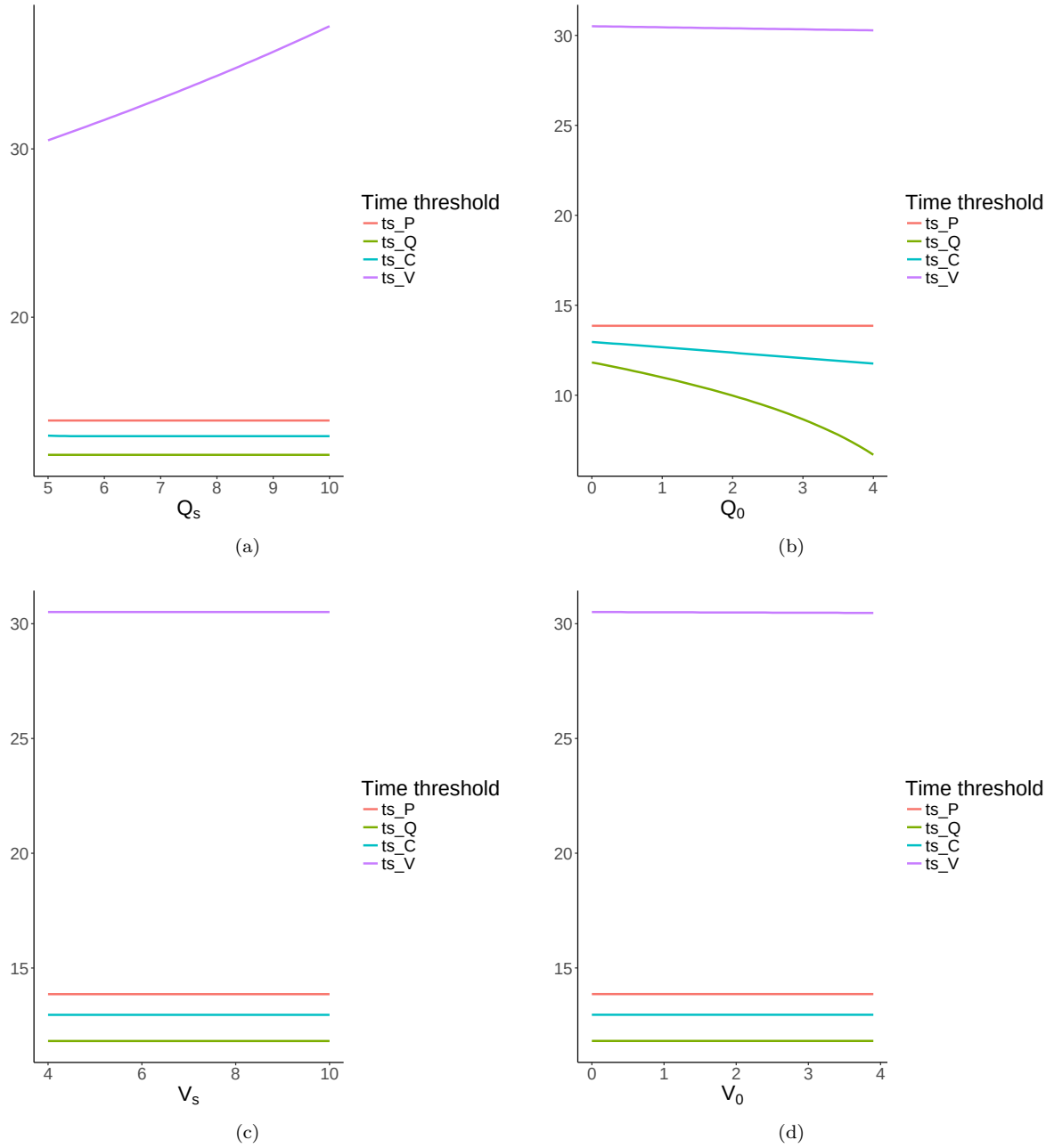

Figure 31: **Time thresholds against parameters in the three-compartment model (3/3).**

Influence of the geometry of the setup chosen for the cell-based simulations on the migration terms

In what follows we illustrate how the choice of the parameters defining the geometry of the cell-based model affects the migration terms. Supplementary Figures 32, 33 show time series resulting when varying crypt and villus lengths and radii respectively by 20% of their default values used in the control simulations presented in Supplementary Figure 1. The two-compartment model was then applied to fit the simulated time courses and the medians of the posterior predictive distribution of the migration terms were calculated; these are presented in Supplementary Figure 34. Whereas an increase in villus length or radius plays a minor role on the migration term, an increase in crypt length or radius causes faster cell migration onto the villus (see Supplementary Figure 34).

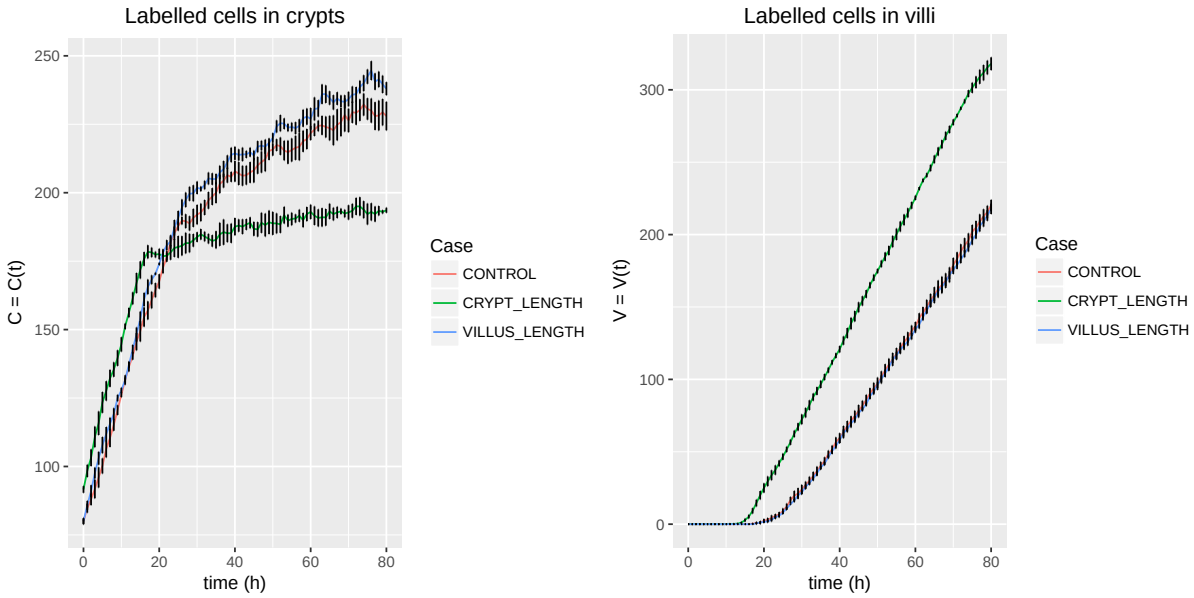

Figure 32: **Time series simulated by applying the cell-based model when varying crypts and villus lengths**. Time series representing average numbers of simulated labelled cells in crypts and villi when the crypt lengths are increased by 20% of their default value, when the villus length is increased by 20% of its default value and with default parameters (control). Averages were calculated from 5 simulations for each condition. Error bars indicate standard errors.

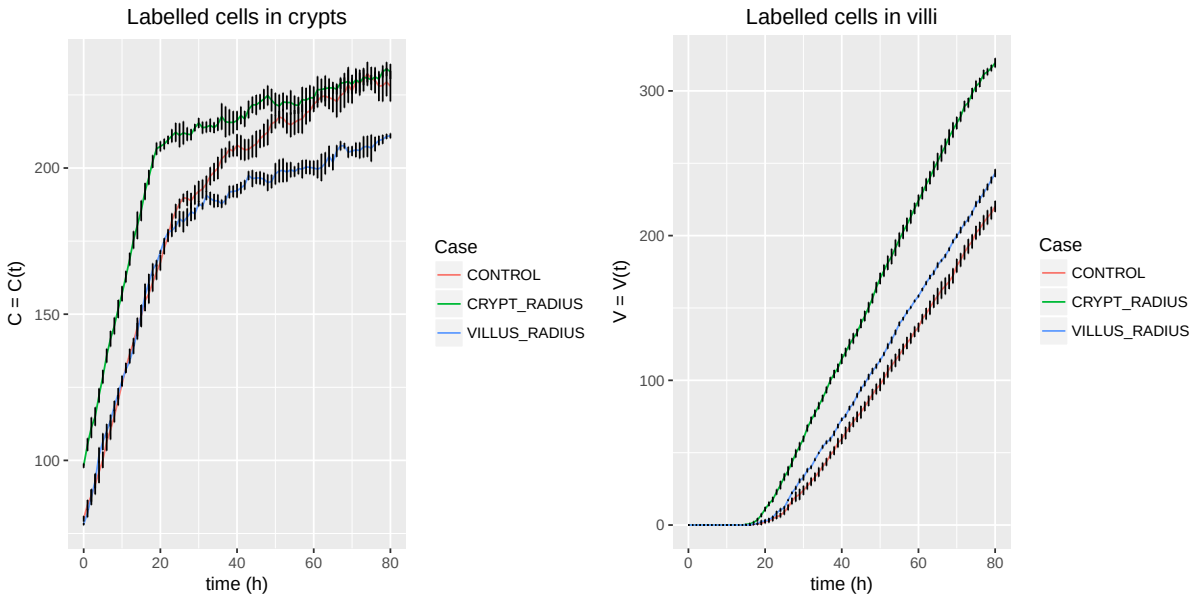

Figure 33: **Time series simulated by applying the cell-based model when varying crypts and villus radii**. Time series representing average numbers of simulated labelled cells in crypts and villi when the crypt radii are increased by 20% of their default value, when the villus radius is increased by 20% of its default value and with default parameters (control). Averages were calculated from 5 simulations for each condition. Error bars indicate standard errors.

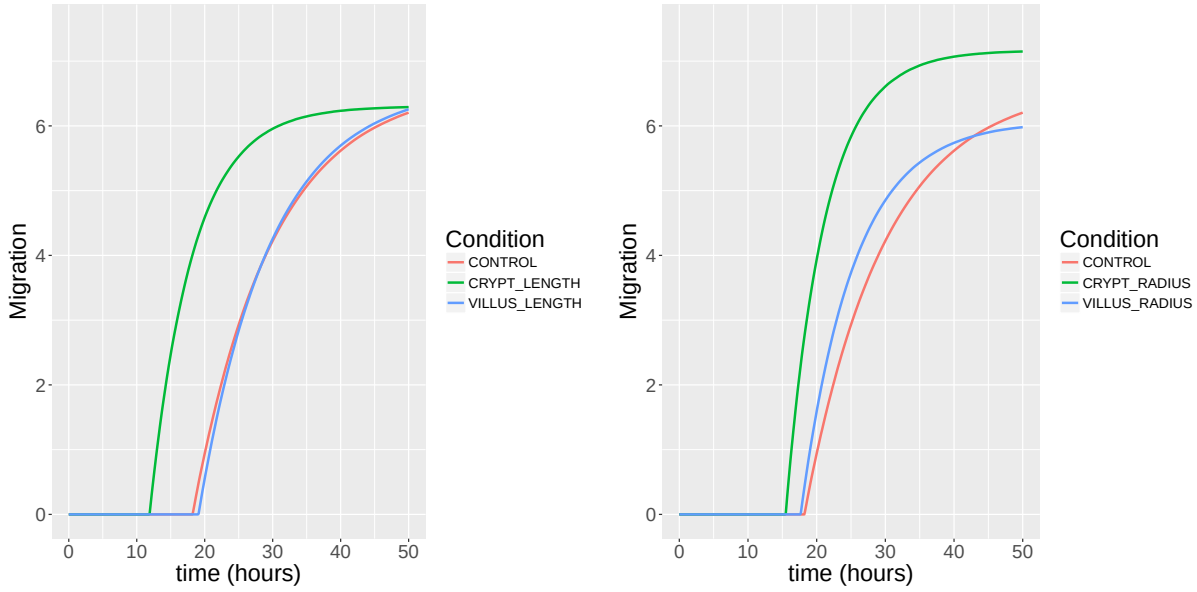

(a) (b)

Figure 34: **Migration terms of the two-compartment model fitted against simulated time courses obtained when varying crypts and villus lengths and radii**. Plots representing the medians of the posterior predictive distribution of the migration terms obtained when fitting the two-compartment model against simulated time courses when varying crypt and villus lengths (a) and radii (b).